Modelling and Path Planning for Additive Manufacturing of Continuous Fiber Composites

by

Suleman Asif

Submitted to the Graduate School of Engineering and Natural Sciences

in partial fulfillment of the requirements for the degree of Master of Science

Sabanci University

July 2018

MODELLING AND PATH PLANNING FOR ADDITIVE MANUFACTURING OF CONTINOUS FIBER COMPOSITES

APPROVED BY:

Prof. Dr. Bahattin Koç .....
(Thesis Supervisor)

Prof. Dr. Mehmet Yıldız .....

Prof. Dr. Halit Süleyman Türkmen .....

DATE OF APPROVAL: 16/7/2018

© Suleman Asif, 2018

All Rights Reserved

Suleman Asif

MFG, M.Sc. Thesis, 2018

Thesis Supervisor: Prof. Bahattin Koç

Abstract

Material-extrusion based Additive Manufacturing (AM) is one of the leading (AM) technologies, which produces three-dimensional (3D) parts by extrusion of molten thermoplastic polymers layer by layer. However, its applications are limited due to the low strength and stiffness of the parts produced by this technology. One of the ways to improve the mechanical properties of the parts is to use a reinforced thermoplastic polymer with a filler such as chopped or continuous fibers. The resulting additively manufactured continuous fiber reinforced thermoplastic (CFRTP) composites could have superior mechanical properties and hence can be used in high-performance applications such as for aerospace and automotive industries.

This thesis is divided into two sections. The first section is related to the modeling of additively manufactured continuous fiber composites for evaluation of the mechanical properties. The current studies for evaluating the mechanical properties of additively manufactured CFRTP composites are based on experimental results. Therefore, there is very limited study available to determine and optimize the process parameters. In this section, a finite element based study is presented to determine the effect of process parameters such as nozzle diameter, layer thickness, volume fraction and infill percentage on elastic properties of additively manufactured CFRTP composite structures.

The second section presents the development of a continuous path planning algorithm for additive manufacturing of continuous fiber composites. The existing path planning algorithms used in material extrusion-based processes cause discontinuities in the material deposition if complex shapes are manufactured. Moreover, they cannot be used for continuous fiber composite printing, since the use of continuous fiber as a reinforcement requires continuous deposition of material throughout the printing process. In this thesis, a novel path planning algorithm has been developed to generate continuous deposition path for 3D printing of continuous fiber composites. The algorithm has been implemented for various complex geometries to generate continues deposition paths for the designed complex parts.

The research conducted in this thesis can expand to the additive manufacturing of CFRTP composites with various reinforcing materials. The developed continuous path planning algorithm can be coupled with the optimized process parameters obtained from modeling results to produce

highly complex shape functional composite parts that could replace the conventional metal parts and processes by providing light-weight solutions for various industrial applications.

Özet

Malzeme ekstrüzyon bazlı katmanlı imalat 3 boyutlu termoplastik polimerin eriyğinden yapılan parçaların katmanlı üretimi için önde gelen yöntemlerdendir. Fakat bu yöntemin uygulanması parçaların düşük dayanıklılık ve sünekliğinden dolayı kısıtlı bulunmaktadır. Parçalarda mekanik özelliklerin iyileştirilmesi doğrultusunda termoplastik polimerin kesik veya sürekli fiberlerle takviyesi sıkcsa kullanılan yötemlerdendir. Sürekli fiberlerle takviye edilmiş termoplastik polimerler'den (CFRPT) üretimin neticesinde mekanik özellikler geliştirlmiş olup ve elde edilen parçalar yüksek performanslı ugulamalarda örneğin uzay ve otomotiv sanayilerinde kullanılmaktadır.

Bu tez çalışması iki bölümden oluşmaktadır. Birinci bölüm katmanlı imalat yöntemi ile üretilmiş sürekli fiber kompozitlerin mekanik özelliklerinin modellemsi ve değerlendirilmesinden oluşmaktadır. Hal hazırdaki katmanlı imalatla üretilen polimer kompozitlerin mekanik özelliklerinin değerlendirilmesi doğrultusunda bulunan çalışmalar deneysel sonuçları baz almaktalar. Bu nedenle bu işlemin değişkelerinin seçimi ve optimize edilmesi üzerinde sınırlı çalışmalar mevcuttur. Bu sekmede, nozel çapı, tabaka kalınlığı, hacim oranı ve doldurucunun yüzdesinin eklemeli yöntem ile üretilen CFRTP malzemesinin elastik özellikleri üzerindeki etkisini anlamak için bir sonlu eleman bazlı araştırması yapılmıştır.

İkinci bölümde, eklemeli yöntem ile üretilen sürekli fiber kompozitlerinin devamlı bir taklım yolu planlamasının algoritması geliştirilmiştir. Ektrüzyon bazlı proseslerde mevcut kullanılan takım yolu planlama algoritmaları karmaşık şekilerde, malzeme birikmesinde devamsızlıklara sebep olmaktadır. Ayrıca, bu yöntemler devamlı fiber kompozitler basmada devamlı fiberlerin takviye olarak işlev yapması devamlı birikme olmasını gerektirdiği nedeniyle kullanılamaz. Bu tezde, yeni takım yolu planlama algoritması sürekli biriktirme takım yolu ile üç boyutlu sürekli fiber kompozit basma için geliştirlimiştir. Algoritma çeşitli karmaşık geometriler üretmek için sürekli biriktirme takım yolllarıyla uygulanmıştır.

Bu tezdeki yapılan araştırma CFRTP kompoziti çeşitli takviye malzemeleriyle eklemeli üretim yöntemi için geliştirilebilir. Modelleme sonuçlarından geliştirilen sürekli takım yolu planlama algoritması, optimizasyon edilmiş proces parametreleri ile tümleşerek karmaşık geometriye sahip

olan işlev kompozit parçaların üretimine yol açacaktır ve dolayısıyla konvansiyonel metal parçaların yerini hafifliğe çozüm getirerek çeşitli sanayilerde kullanılacaktır.

Acknowledgments

First of all, I would like to thank Sabanci University and Faculty of Engineering and Natural Sciences for giving me the opportunity to study and showcase my research abilities. I am proud to be among the first graduates of the Manufacturing Engineering program at Sabanci University.

I would especially express my gratitude to my advisor Prof. Bahattin Koc for his support, assistance, and introduce me to novel research ideas for my thesis. His guidance and encouragements were very valuable to me during my research work. I would like to thank Ferdows Afghah, Cem Dayan, and Kerem Dortkasli from Koc group for assisting me during my research. I am also grateful to Asst. Prof. Adnan Kefal from ITU for helping me in Finite Element Model.

I would like to thank the members of the Pakistani community in Sabanci University, especially my roommate Rayan Bajwa, for making my stay feel such as home during my master's program. I am also grateful to my Turkish and international friends including Hazal Goktas, Nima Zoghipour, and Pouya Zoghipour for making my experience enjoyable one.

Finally, I would like to thank my father and sister for their emotional support during my studies. Their expectations are the motivation for me to be successful in my career.

Dedicated to the loving memory of my mother

Contents

1. Introduction 1

1.1 Additive Manufacturing (AM) 1

1.2 Material Extrusion 1

1.3 Additive Manufacturing of thermoplastic composites using Fused Deposition Modeling .. 2

1.4 Continuous path planning for Additive Manufacturing 7

1.5 Objectives of this thesis 9

2. Modeling of additively manufactured continuous fiber reinforced thermoplastic composites 10

2.1 Introduction 10

2.2 Modelling of geometries 11

2.2.1 Nozzle diameter 12

2.2.2 Layer thickness 12

2.2.3 Volume fraction 12

2.2.4 Infill percentage 12

2.3 Analytical model 14

2.4 Finite element analysis 15

2.5 Results and comparison with analytical model 16

2.6 Discussion 22

3. Continuous path planning for additive manufacturing of continuous fiber composites 23

3.1. Methodology 23

3.2.1. Raster filling methodology 23

3.2.4. Determination of extremum points along the scanning direction 26

3.2.5. Deposition path generation 27

3.2.6. Avoiding deposition outside the part 30

3.2.7. Avoiding the over-deposition 33

3.2.8. Filling of boundary and moving to the next layer 35

3.3. Results 36

3.3.1. Comparison with commercial software 36

3.3.2. Implementation on 3D printer 37

4. Conclusion and future work 38

5. References 40

List of figures

Figure 1. 1. Schematic diagram of coaxial printing process for continuous fiber composites 4
Figure 2. 1. Coaxial CFRPT printing and composite structure with unit cell……12

Figure 2. 2. Unit cells with different infill percentages (a) Low infill percentage (b) High infill percentage 13
Figure 2. 3. The visual representation of geometries by changing different process parameters. 14
Figure 2. 4. Axis used for analysis..... 16
Figure 2. 5. Comparison of finite element results with analytical models. 17
Figure 2. 6. Effect of nozzle diameter on elastic modulus of continuous fiber composites 18
Figure 2. 7. Effect of layer thickness on elastic modulus of continuous fiber composites..... 18
Figure 2. 8. Effect of volume fraction on elastic modulus of continuous fiber composites 19
Figure 2. 9. Effect of infill percentage on elastic modulus of continuous fiber composites 19
Figure 2. 10. Effect of nozzle diameter on shear modulus of continuous fiber composites..... 20
Figure 2. 11. Effect of layer thickness on shear modulus of continuous fiber composites 20
Figure 2. 12. Effect of volume fraction on shear modulus of continuous fiber composites..... 21
Figure 2. 13. Effect of infill percentage on shear modulus of continuous fiber composites 21

Figure 3. 1. (a) Bounding box with corner points of the curve (b) Deposition of points by intersection of lines…….25

Figure 3. 2. The curve containing the maximum and minimum points..... 27
Figure 3. 3. Obtaining the curve segment for ReturnPoint function..... 28
Figure 3. 4. Obtaining the curve segment for deposition along the curve 31
Figure 3. 5. Continuous filling of a complex concave geomerty..... 32
Figure 3. 6. Explanation of continuous path planning algorithm on a complex geometry..... 34
Figure 3. 7. Filling of a complete 3D model (a)Filling inside internal offsetted curve in first layer (b) Plotting the boundary of first layer (c) Filling along the internal offsetted curve in the second layer (d) Raster pattern scanning along y-direction in internal offsetted curve in second layer (e)Filling of boundary of second layer (f)Filling of a complete 3D model . **Error! Bookmark not defined.**

Figure 3. 8. Filling of a complex concave shape geometry (a) Using continuous path planning algorithm (b) using commercial software 36
Figure 3. 9. Filling of a fidget spinner (a) Using continuous path planning algorithm (b) using commercial software 37
Figure 3. 10. Implementation of algorithm on a commercial printer (a) Complex concave geometry (b) Fidget spinner 38

List of tables

Table 2. 1. Parameters used for analysis 16

1. Introduction

1.1 Additive Manufacturing (AM)

Additive Manufacturing (AM) is an emerging manufacturing technique in which parts are produced layer by layer, directly from Computer Aided Design (CAD) models [1]. This process manufactures part by adding material as opposed to machining or subtractive manufacturing in which parts are produced by removing material from a stock [2]. The terms layered manufacturing, 3D Printing, and Rapid Prototyping are also used for AM. The significance of AM is its ability to produce highly complex parts with minimum waste of material, which makes it a more favorable manufacturing technique as compared to conventional processes [3]. The design freedom and flexibility associated with AM helps the users to develop and customize their parts according to their needs [4]. AM can be used to produce efficient, stronger, and light-weight functional parts for various industrial applications. These advantages of AM have resulted in huge commercial success of the technology. The market for AM is growing at a rapid pace, and it is expected to reach 13 billion US dollars by the end of 2018. AM processes have found applications in automotive, aerospace, fashion, art design, and biomedical applications [5]. The major drawbacks of AM process are relatively long build time, lower mechanical properties, low-quality surface finish, and post-processing of manufactured parts.

1.2 Material Extrusion

Material-extrusion based AM processes are the most commonly used AM techniques which manufacture 3D parts by melting and extrusion of thermoplastic polymer through a nozzle onto a print bed layer by layer. It is commercialized by Stratasys company and commonly referred to Fused Deposition Modeling (FDM). In this process, parts are manufactured layer by layer, in which completion of one layer, the printhead moves upwards along z-direction by a distance equal to the layer thickness, and the next layer is deposited. This process continues until the part is completely printed [6]. The most commonly used thermoplastics materials in this process are Polycaprolactone (PCL), Polylactic acid (PLA), Acrylonitrile butadiene styrene (ABS) and Nylon. The material can be fed to the nozzle in filament form or directly through plastic pallets. The important printing parameters are extrusion temperature, feed rate and nozzle diameter [7]. The

process was first developed by Stratasys in 1990. With the expiration of its patent, FDM has gained widespread popularity as one of the leading AM technologies [8]. The reasons for the success of the technology have been the low cost of machines, easily available raw materials, and the simplicity of the printing process [9]. The emergence of open-source development communities such as RepRap and Fab@Home have played a key role in the popularity of the technology [10]. The main disadvantages associated with FDM process are poor mechanical properties of manufactured parts, poor surface finish, long build time, and post-processing requirements such as removal of support material [11][12].

1.3 Additive Manufacturing of thermoplastic composites using Fused Deposition Modeling

To improve the mechanical properties of the FDM parts, thermoplastic materials have been reinforced with either short fiber or continuous fibers. Until now, several studies have been conducted by reinforcing thermoplastic materials with short fibers to enhance the mechanical properties. Zhong *et al*. [13] modified the ABS filament with short glass fibers, plasticizer, and compatibilizer. The reinforced filament was used as a feedstock material for FDM printer. The mechanical properties of ABS filament were enhanced, but issues such as control of extrusion force and potential tool wear were observed. Shofner *et al.* [14] reinforced ABS matrix with single wall carbon nanotubes and vapor grown carbon fibers composites using FDM. Tensile tests were performed after printing with modified feedstock material and results exhibited tensile strength and Young's modulus were increased considerably. Nikzad *et al.* [15] introduced iron and copper metal particles in ABS material and studied the thermal and mechanical properties of printed composite samples. The fiber content was controlled by centrifugal mixing and the results of the tests showed significant improvement in thermal and mechanical properties. Tekinalp *et al*. [16] reinforced ABS by introducing the short carbon fiber in the range of 10-40% volume fraction. It was found that the fibers were highly oriented towards printing direction. The results of tensile tests showed remarkable improvement in tensile modulus. However, the tensile strength was marginally increased. The high porosity in the printed samples was the major issue in printed samples. Ning *et al*. [17] produced modified ABS filament by mixing of ABS with short carbon fiber of varying content and length. There was a promising improvement in tensile and flexural

properties. However, an increase of fiber content resulted in an increase of porosity, which limits the mechanical properties at higher wt% of fiber. Quan *et al*. [18] designed the 3D orthogonal preforms by controlling yarn orientation and sheet alignment. This was followed by addition of short carbon fibers as reinforcement in the ABS preform. The compressive behavior reinforced performs was analyzed. However, poor interfacial bonding of ABS and carbon fibers was observed. Carneiro *et al.* [19] evaluated the potential of polypropylene as a feedstock material for the FDM process. PP was reinforced with short glass fibers and effect of parameters such as filament orientation and layer thickness were evaluated in comparison with pure PP samples. Ferreira *et al.* [20] performed the mechanical characterization of PLA specimen reinforced with 15 wt% short carbon fibers. The tensile and shear properties were evaluated, and promising improvements were observed. However, poor interfacial bonding between PLA and carbon fibers was a major issue with the proposed method. Girdis *et al*. [21] introduced short carbon fiber and graphene into ABS and PLA to produce modified filaments. Composite specimens were printed using a commercial 3D printer and their mechanical and electrical properties were observed. It was noted that an addition of only 2 wt% short carbon fibers had a significant effect in mechanical properties. In addition, the inclusion of graphene also improved the conductivity of PLA.

The reinforcement of short and nanofibers in thermoplastics have provided promising results as far as the improvement in mechanical properties is concerned. However, the reinforcement with continuous fibers can be more suitable for aerospace and automotive applications because of better control of fiber orientation in continuous fiber composite can provide better directional properties to the parts [22][23].

The AM of continuous fiber reinforced thermoplastic (CFRPT) composites has been an active area of research in recent years. In this process, both thermoplastic polymer and continuous fiber are fed simultaneously into nozzle in (CFRPT) composites printing process as shown in Figure 1.1.

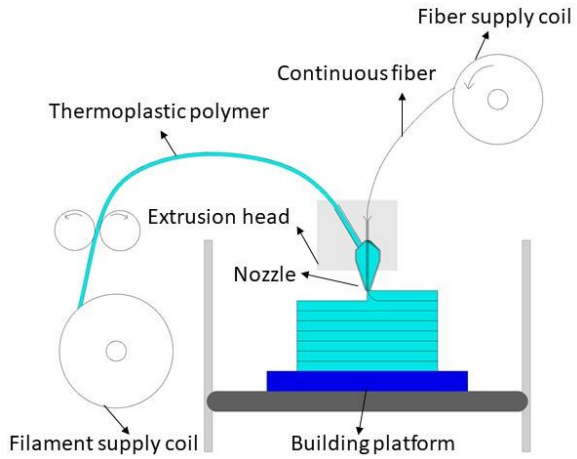

Figure 1. 1. Schematic diagram of 3D printing process with continuous fiber composites [24]

Matsuzaki *et al.* [25] developed a novel method for 3D printing of CFRTP composites using FDM. PLA and continuous fiber were supplied separately to the nozzle of a 3D printer. The reinforcement was done using carbon fiber and jute fibers. The samples were printed according to JIS standards, and tensile and flexural tests were performed to evaluate the improvement of mechanical properties in comparison with pure PLA samples. According to the results, there was a significant improvement in the properties of carbon fiber reinforced PLA samples. However, the increase in strength of Jute reinforced samples was not very significant because of the degradation of fiber-matrix interactions. The 3D printed composite samples were termed as "Composite 2.0". Klift *et al.* [26] performed a study to evaluate the capabilities of Mark One 3D printer, which is the first commercial 3D printer capable of printing continuous fiber composites. Nylon is the matrix material that is reinforced with carbon fiber. Three different types of samples were printed, each consisting of 10 layers, to evaluate the mechanical properties. The first type of sample was pure Nylon, i.e. none of the layers were reinforced with carbon fiber. The second type of sample had two carbon fiber layers in the middle, and thus it was termed as 2CF specimen. The third type had six layers of fiber, and it was referred to as 6CF. The volume fraction of the samples was determined, and the tensile test was performed to observe the mechanical properties, and to see whether the composite samples live up to the rule of mixtures of composites. The 2CF and 6CF specimen showed promising improvement in mechanical properties by reinforcement with carbon fiber. However, because of discontinuities in fibers and void formation, the specimen could not live up to rule of mixtures completely. Li *et al.* [27] proposed a novel method to solve the of weak

bonding between resin and fiber in method presented by Matsuzaki *et al.* [25] PLA was used as matrix material which was reinforced with the carbon fiber. A conical nozzle was used to produce uniform mixing of resin and fiber. The surface modification of carbon fiber was performed, as a preprocessing stage, to improve the adhesion of carbon fibers with PLA. Tensile and bending test were performed on pure PLA samples, carbon fiber reinforced PLA samples, and modified carbon fiber reinforced PLA samples. The results showed unmodified carbon fiber reinforced PLA samples had significantly higher tensile and flexural strength values in comparison with the pure PLA samples. The modified carbon fiber reinforced PLA samples showed considerably higher flexural strength as compared to samples reinforced with original carbon fibers. It shows the effectiveness of performing preprocessing modification of carbon fibers in improving the interfacial strength between PLA and carbon fiber. Furthermore, a path control method was developed to print complex geometries including hollow-out aerofoil, a unidirectional flat part, and a circular part. Nakagawa *et al.* [28] proposed a novel method to produce continuous carbon fiber composites. ABS was the matrix material that was reinforced with carbon fibers. Two nozzles with different diameters were used to determine the effect of nozzle diameter. Instead of using coaxial printing method, the carbon fibers were sandwiched between upper and lower layers of ABS. The process worked in such a way that after printing of lower layers of ABS, carbon fibers was put and thermally bonded using heating pin before the upper layer of ABS were printed. In addition, some samples were also thermally bonded using a microwave to understand the difference between both methods. Tensile and flexural tests were conducted on the specimen to determine the effectiveness of the proposed technique. The results showed considerable improvement in the mechanical properties of the composite specimen as compared to pure ABS. In addition, it was observed that there was not much difference between the results obtained from test specimen thermally bonded by heating pin and microwave oven. So, it was concluded that microwave could be successfully used for thermal bonding between matrix and fiber layers. Bettini *et al*. [29] printed CFRTP composites by modification of a commercial 3D printer Blue Tek Strato, PLA was the matrix material that was reinforced with aramid fibers because to their high toughness and stiffness in comparison with glass and carbon fibers. The extrusion rate was kept low during printing to avoid mismatch in feeding rate of plastic and fiber. Tensile tests were performed on the 3D printed composite samples. The results show notable enhancement in the mechanical properties of composite samples. Tensile strength and elastic modulus were increased 3 and 6 times,

respectively, as compared to pure PLA samples. To extend the application of the technique, path planning for some parts with complex geometries was also done to print a tube, a rectangular cross-section, a T beam and a complicated rib-shaped part. Zhang *et al.* [30] proposed the composition of a continuous carbon fiber composites 3D printing system. The first stage of the system was slicing of a 3D model. The control and monitoring of the printing process were studied. In addition, the 3D model digital expression and identification of breakpoint for path planning for complex 3D models were also analyzed. It was concluded that the system could replace the conventional manufacturing systems. Vaneker *et al.* [31] proposed a pultrusion based method for 3D printing of continuous fiber composites. The material used as a raw material was commingled yarn which contains polypropylene (PP) as the matrix that is reinforced with E-glass. A cutting device was also incorporated in the system, and a novel deposition strategy was developed. The results showed a remarkable increase in flexural modulus as compared to pure PP. However, the void presence in the samples was a major issue in the proposed technique. Tian *et al.* [24] performed 3D printing of CFRTP composites using PLA and carbon fiber. The interface and performance of 3D printed samples were investigated. The Melt Flow Index of PLA was studied to determine the effect of temperature on the melting viscosity. The effect of different printing parameters such as temperature, pressure and fiber content on the flexural properties was studied, and optimized parameters were determined. The flexural tests showed promising results using the optimized parameters. Yamawaki *et al.* [32] developed a new 3D printer for printing of CFRTP composites. Two different extruders were used that separately supplied the matrix and fiber. Nylon was chosen as matrix material while continuous carbon fibers were reinforcement. The composite samples of 2, 3 and 4 layers were printed with an extrusion temperature of 250°C, a feed rate of 60 mm/min, and a volume fraction of 50%. The samples were post-processed using annealing and hot press treatment to observe the effect in mechanical properties. Tensile tests were conducted, and it was concluded that the hot press treatment significantly improved the tensile strength and Young's modulus of the composite specimen. However, annealing had a marginal effect on mechanical properties. Dickson *et al.* [33] studied the mechanical properties of continuous carbon, Kevlar and glass fiber reinforced Nylon composites printed using Mark One commercial 3D printer. The effect of volume fraction and fiber type were studied, and the results of tensile and flexural tests determined that the samples reinforced with carbon fiber provide the best mechanical properties. The inclusion of fibers significantly increased the strength of the samples, however, the effect was

not observed to be linear with increase in fiber content. The inclusion of air in the samples was concluded to be the major issue limiting the strength of the composite parts. Hou *et al.* [34] presented a novel 3D printing process for manufacturing of continuous fiber reinforced composite lightweight structures. Cross lap and panel-core lap design methodologies were presented to print the composite structures with complex geometries. The printing device was incorporated with a robotic arm with 6 degrees of freedom. PLA was used as matrix material which was reinforced with Kevlar fiber. The process parameters were varied, and fracture modes were studied during compression loading. It was concluded that the proposed method is capable of producing lightweight composite structures with excellent mechanical and functional properties. Yang *et al.* [35] developed a novel extrusion head for 3D printing of CFRTP composites. ABS was chosen as matrix material while carbon fiber was used as reinforcement. Composite specimen with 10% volume fraction were printed. The mechanical tests showed significant improvement in tensile and flexural strength. The results were closer to the composite specimen manufactured using an injection molding process. However, the interlaminar shear strength was lower because of weak interface bonding between fiber and matrix.

These studies have shown promising improvement in mechanical properties in comparison with pure thermoplastic samples. However, there is no control of fiber position in the nozzle which causes random mixing of polymer and fiber in the nozzle and results in poor adhesion between them. The system also needs to be designed in such a way that the fiber lies directly in the center of the nozzle to ensure that the thermoplastic polymer is properly diffused into the fiber from all sides using a coaxial printing process in which more than one materials are extruded simultaneously through a nozzle along a common axis. Moreover, these studies are only limited to the printing of ASTM test standard specimen and simple shape parts because the use of continuous fiber as a reinforcement requires continuous deposition of material throughout the printing process. There is a need for a continuous path planning algorithm to print complex shape parts for industrial applications.

1.4 Continuous path planning for Additive Manufacturing

In FDM based systems, path planning is the process of obtaining point locations where extruder is guided to deposit the material to fill layers. The path planning for FDM resembles that of CNC

pocket milling, in which material is removed instead [36]. Most commonly used patterns in pocket milling are spiral, zigzag and contour offset [37]. The spiral pattern is more frequently used in pocket milling since it provides continuous removal of material from the workpiece. However, path planning for FDM can become much more complicated because, in a pocket milling process, it is not that important how the material is removed. The air cut phase during the pocket milling is not desirable in FDM since the spindle in pocket milling can keep rotating during air cut, but on the other hand, it would require the extrusion to pause and resume continuously during FDM process. It results in discontinuities in the material deposition, which can affect the strength of the part. Moreover, the choice of the filling pattern has a direct effect on the strength of the part and surface finish during the FDM process. Several filling patterns are used such as raster $0^0/90^0$, raster $0^0/45^0$, triangular, and hexagonal. The cross-weaving patterns are more commonly used because they provide even distribution of strength inside a layer. However, these patterns produce sharp corners and turns that affect the part accuracy. Therefore, in normal practice the interior region of the layer is filled first, followed by plotting of boundary. This helps in providing a smooth surface finish and accuracy [38].

The existing path planning algorithms used in the FDM process causes discontinuities in the material deposition if complex shapes are required to be printed. However, they cannot be used for continuous fiber composite printing, since the use of continuous fiber as a reinforcement requires continuous deposition of material throughout the printing process. Discontinuities in the material deposition is an issue in path planning for normal FDM process as well. Discontinuities can severally compromise the mechanical strength of the part. Furthermore, they can cause under-deposition or over-deposition at the start or stop locations and hence cause rough surfaces or deformed shapes.

Until now, most of the work related to the generation of a continuous path is limited to machining processes[39][40][41][42][43][44]. However, some work has also been done in the field of path planning for additive manufacturing. Sheng *et al*. [45] presented a decomposition-based method, in which a 2D polygon is partitioned into a set of sub-polygons and deposition path for each sub polygons is generated. However, connectivity of the deposition paths was a major issue in some cases. Dwivedi and Kovacevic [46] proposed a method based on the subdivision of a 2D polygonal section into a set of monotone polygons. The 2D contour was divided into sub-polygons, and path

for each of the sub-polygons was generated individually and connected to create a continuous path. Bertoldi *et al.* [47] employed the Hilbert space-filling curve generation method to generate continuous path planning. Ding *et al.* [48] proposed a method to generate optimal deposition paths for the Wire Arc Additive Manufacturing (WAAM). The method employs a divide-and-conquer strategy to divide 2D geometries into a set of convex polygons. Then an optimal scan direction is determined, and a continuous deposition path is generated for each polygon. Finally, all disconnected sub-paths are joined to form a closed curve. The algorithm successfully minimizes the start and stop points and produces a good surface accuracy of the end parts. Zhao *et al.* [49] presented a novel path planning algorithm for continuous filling of a 2D region using connected Fermat spirals. Khoda *et al.* [50] presented a novel path planning algorithm for tissue scaffold design with controllable heterogeneous architecture. Jin *et al.* [36] developed a non-retraction path planning approach using "go and back" strategy to generate a continuous deposition path, in which the start point is connected to the endpoint in each sub-region. However, there was an issue related to under-deposition and over-deposition in the deposition path.

The algorithms presented in the literature apply to the only certain type of geometries and contain issues such as under-deposition, over-deposition and movement of the extruder to next layer after filling one layer. Some of them are not applicable for raster path planning pattern and hence cannot be used for 3D printing of CFRTP composites that provide directional properties. Hence, there is need of a continuous path planning method that can generate a deposition path without any under-deposition and over-deposition, and with better moving strategy from one layer to the next one.

1.5 Objectives of this thesis

Since the available studies for evaluation of the mechanical properties of additively manufactured CFRTP composites are based on experimental results, there is very limited study available for determining and optimizing the process parameters. Therefore, a comprehensive analysis is required to study the effect of process parameters such as nozzle diameter, layer thickness, infill percentage and volume fraction on effective elastic properties of CFRTP composites. Moreover, to be able to use those parameters to produce a complex shape parts, a continuous path planning algorithm is needed to generate a deposition path for any singly connected curve shaped object.

The main objective of this thesis is for modeling and path planning of continuous fiber reinforced thermoplastic composite structures.

Chapter 2 presents a finite element study to determine the effect of parameters such as nozzle diameter, layer thickness, infill percentage and volume fraction on elastic properties of additively manufactured continuous fiber reinforced thermoplastic composite structures.

Chapter 3 presents a novel path planning algorithm to generate continuous deposition path for 3D printing of continuous fiber composites. The algorithm has been implemented and applied to generate deposition paths for complex shape parts.

2. Modeling of additively manufactured continuous fiber reinforced thermoplastic composites

In this chapter, a finite element analysis of additively manufactured continuous fiber composites is given. The geometries were modeled, and finite element analysis was used to study the effect of different parameters on mechanical properties of 3D printed continuous fiber composites with different matrix and fiber combinations.

2.1 Introduction

In this thesis, a novel coaxial FDM method is developed in which more than one materials are extruded simultaneously through a coaxial nozzle along a common axis as shown in Figure 2.1. The coaxial FDM based printing of continuous fiber composites can have several parameters such as nozzle diameter *dia*, layer thickness *LT*, infill percentage *IP* and volume fraction V_f. The mechanical properties of 3D printed continuous fiber reinforced thermoplastic composites are very contingent on the choice of these parameters.

The current studies for evaluating the mechanical properties of CFRTP composites are based on experimental results. Therefore, there is very limited work available for evaluating the effects of parameters on the resultant parts. Matsukazi *et al.* [25] printed CFRTP composites by modifying a commercial 3D printer but stressed the need for a comprehensive numerical model to effectively study the mechanical properties. Currently, there is no numerical study available for the modeling of 3D printed CFRTP composites using coaxial FDM process shown in Figure 2.1.

This chapter presents a comprehensive analysis of the effect of process parameters such as nozzle diameter, layer thickness, infill percentage and volume fraction on the effective elastic modulus of CFRTP composites in different directions. The geometries were modeled based on unit cells, and finite element analysis was applied to compute effective elastic modulus using commercial software, Ansys. The unit cell approach has been successfully applied in the modeling of 3D printed scaffold structures [51]. Different material combinations have been used for analysis including PLA, Nylon, and ABS as the matrix material and carbon, glass, and Kevlar fibers as reinforcement. These combinations are based on common choices of matrix and fiber used in 3D printing of CFRTP composites.

2.2 Modeling of geometries

Figure 2.1 shows the geometry of CFRTP composites modeled. The matrix is shown in grey color while fiber is represented in red color. The structure consists of circular struts reinforced with circular fibers. The complete structure can be created by repeating the unit cell in 3 dimensions. The unit cell is a smallest possible structure in the material that contains all the properties of the whole structure.

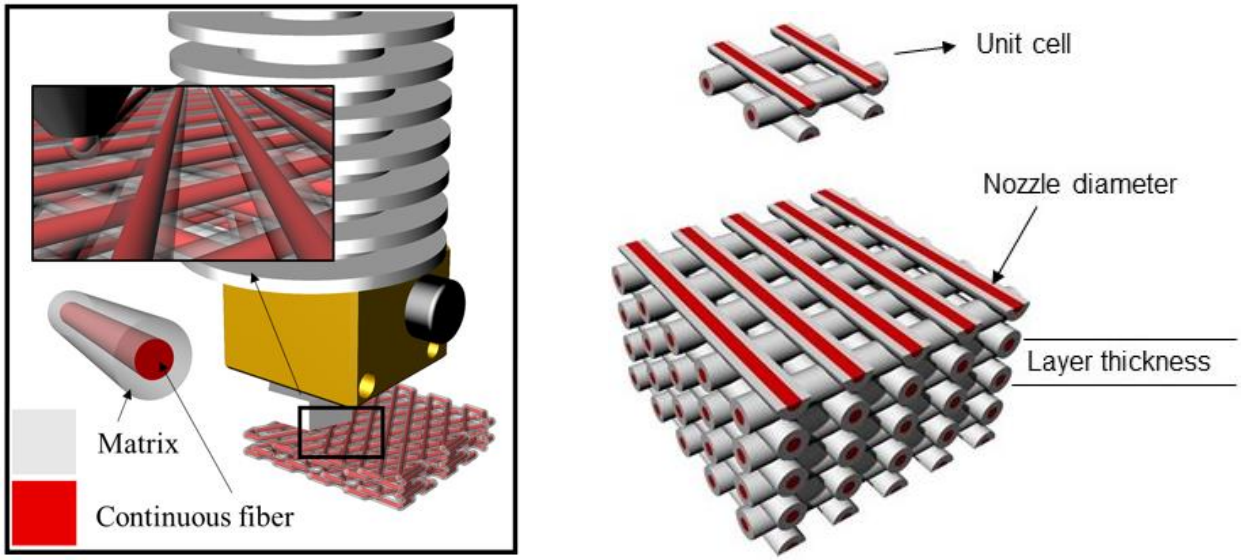

Figure 2. 1. Coaxial CFRPT printing and composite structure with unit cell

The parameters are defined as follows.

2.2.1 Nozzle diameter

It is the diameter of the coaxial nozzle through with matrix and fiber are simultaneously extruded.

2.2.2 Layer thickness

The layer thickness is the distance between two consecutive layers.

2.2.3 Volume fraction

Since both the struts and fibers are considered circular in cross-section, the volume fraction of the whole composite structure can be calculated by the ratio of the cross-sectional areas of matrix and struts.

Volume fraction $= \frac{V_f}{V_s} = \frac{A_f}{A_s}$

Where V_f, V_s, A_f and A_s are fiber volume, strut volume, fiber area and strut area respectively.

2.2.4 Infill percentage

Infill percentage is the ratio of volume of the unit cell divided by the volume of box enclosing the unit cell, which is termed as bounding box.

Infill percentage = $\frac{volume\ of\ the\ unit\ cell}{volume\ of\ bounding\ box}$

Figure 2.2 shows two unit cells with corresponding bounding boxes. Both the unit cells have the same nozzle diameter, layer thickness and volume fraction but different infill percentages. Clearly, the unit cell in Figure 2.2(b) occupies more fraction of volume of bounding box than that of Figure 2.2(a), and hence it has higher infill percentage.

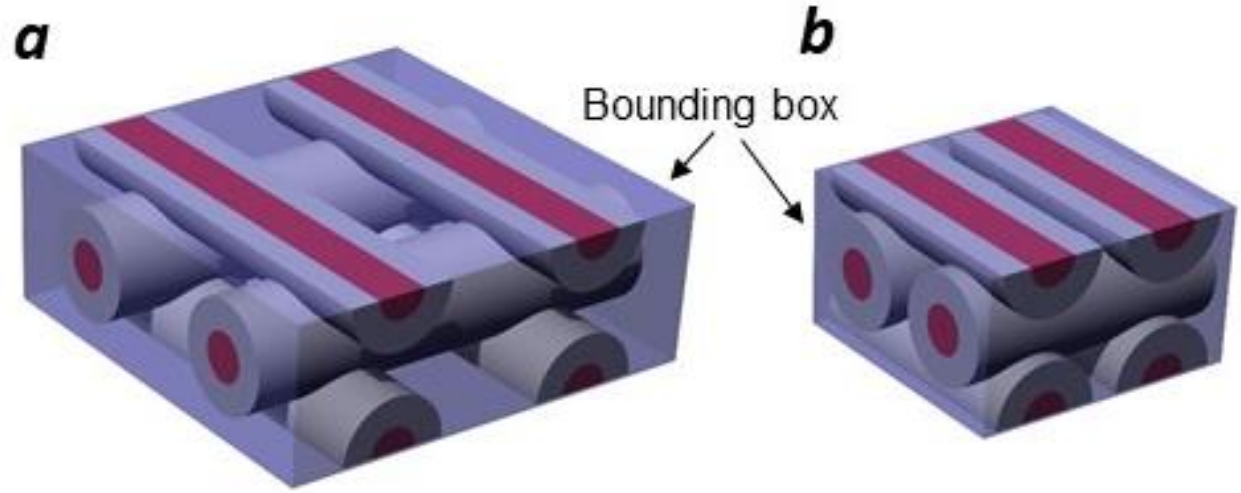

Figure 2. 2. Unit cells with different infill percentages (a) Low infill percentage (b) High infill percentage

The overall geometry of the 3D printed composite structure is dependent on process parameters such as nozzle diameter, layer thickness, infill percentage and volume fraction. The variation in these parameters can significantly alter the effective elastic properties of the composite structure. The visual representation of geometries by a change in parameters is shown in the Figures 2.3.

- Small nozzle diameter
- Small layer thickness
- Low volume fraction
- Low infill percentage

- Large nozzle diameter
- Large layer thickness
- Low volume fraction
- Low infill percentage

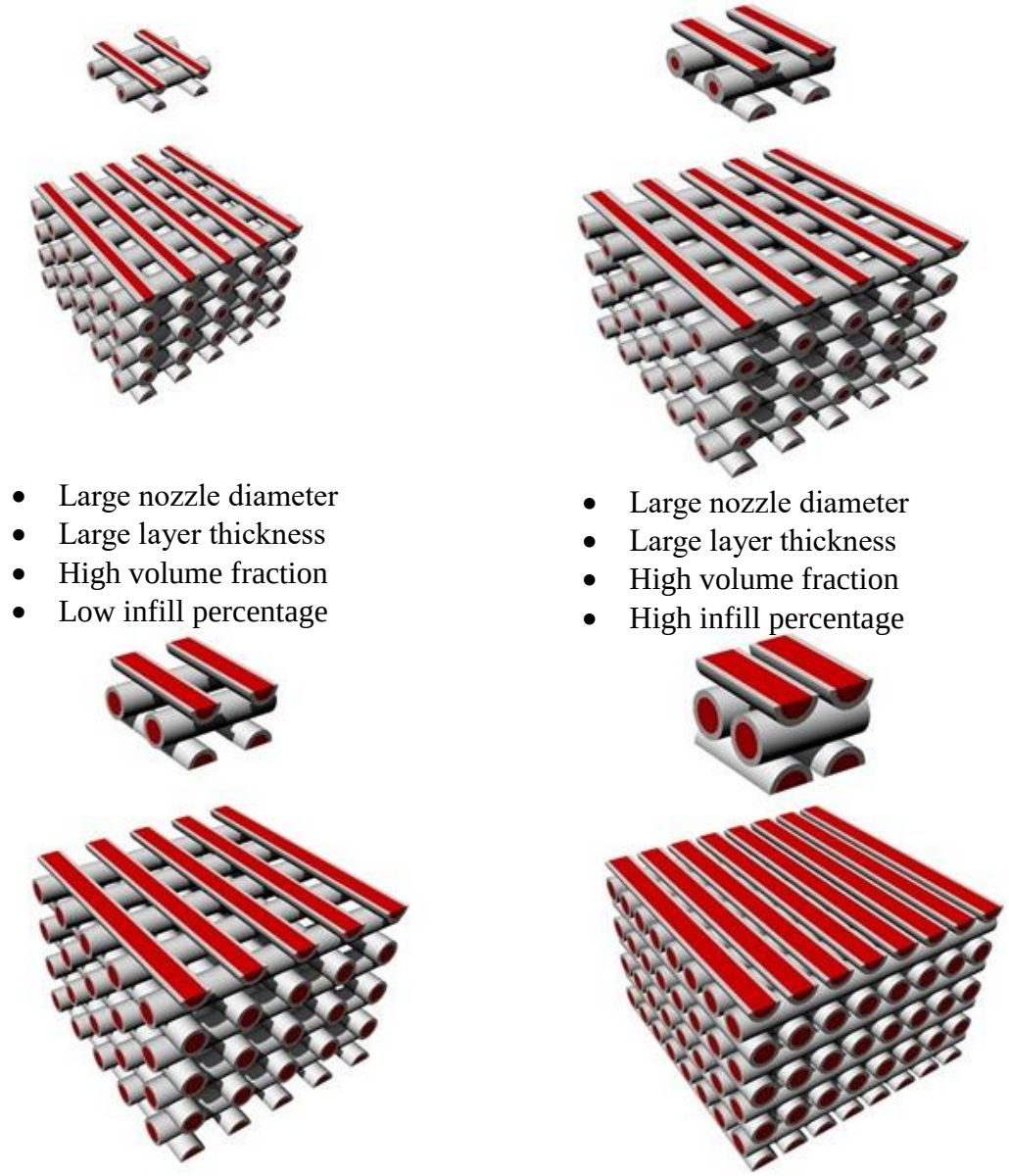

Figure 2. 3. The visual representation of geometries by changing different process parameters

2.3 Analytical model

The effects of process parameters such as nozzle diameter, layer thickness, infill percentage and volume fraction on the elastic properties of CFRTP composites are determined using finite element analysis. The results obtained from the finite element analysis simulations need to be confirmed using the analytical models. The Voigt and Reuss's bounds have been employed in this study for confirmation of the results. The bounds are most commonly used in solid mechanics to provide

lower and upper bounds of the values of elastic properties to predict the properties of composite structures.

The Voigt model is commonly used as the upper bound, and it is based on the assumption that when the load is applied along the fiber direction, both fiber and matrix have similar deformation causing an iso-strain condition in the composite structure. On the other hand, the Reuss model is referred as the lower bound, and it is based on iso-stress assumption.

$$E_{Voigt} = \sum_{j=1}^{n} V_j E_j$$

$$\frac{1}{E_{Ruess}} = \sum_{j=1}^{n} V_j \ E_j^{-1}$$

Where V_j is denoted as the volume fraction of the corresponding matrix and fiber phases. A finite element results should then be bounded between those lower and upper values from analytical models.

2.4 Finite element analysis

The analytical models take only the elastic modulus and volume fraction as the variables, and hence they cannot be used to determine the elastic properties when variables such as nozzle diameter, layer thickness, infill percentage and volume fraction are involved in the calculation. Therefore, a finite element analysis was developed using Ansys Workbench to calculate the effective elastic modulus in a different direction. The axis used for the simulation are shown in Figure 2.8. The Young's Modulus along 1-,2- and 3-direction are denoted as E_1, E_2, and E_3 respectively. While the shear modulus along 12-,13- and 23-direction are denoted as G_{12}, G_{13}, and G_{23} respectively. The finite element analysis is based on the following assumptions.

- Both fiber and matrix are assumed to be linearly isotropic materials.
- Perfect bonding exists between the matrix and reinforcing fibers.
- The shape or diameter of the struct remains same after extrusion. For example, the phenomena of die swell does not exist.

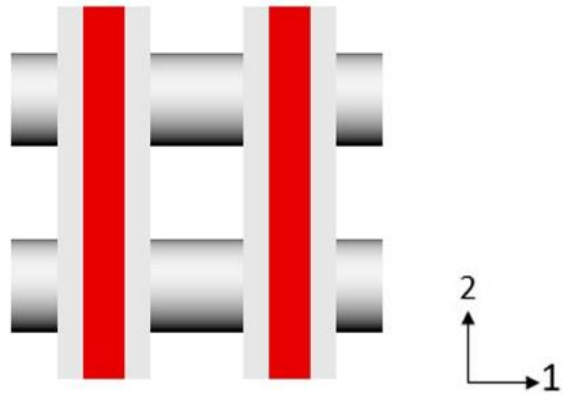

Figure 2. 4. Axis used for analysis

During analysis, the stress was applied on unit cell models, and the strain was calculated for the results of the analysis. The elastic modulus is calculated as the ratio of stress over strain. The results are presented in Tables 2.2-2.5 for the parameters given in Table 2.1 such as matrix and reinforcement materials, nozzle diameter *dia*, layer thickness *LT*, volume fraction V_f, and infill percentage *IP*.

Table 2. 1. Parameters used for analysis

Matrix	Reinforcement	Nozzle diameter (mm)	Layer thickness (*dia* fraction)	Volume fraction (%)	Infill percentage (%)
PLA	Carbon	0.4	0.7	20	70
Nylon	Kevlar	0.6	0.8	30	80
ABS	Glass	0.8	0.9	40	90

2.5 Results and comparison with the analytical model

The results of finite element simulation have been compared with an analytical model for verification. The comparison the average values of elastic modulus have been used to see if they lie within the range of lower and upper bound of values of elastic properties of composites. The results of the comparison with analytical models are shown in Figure. 2.5.

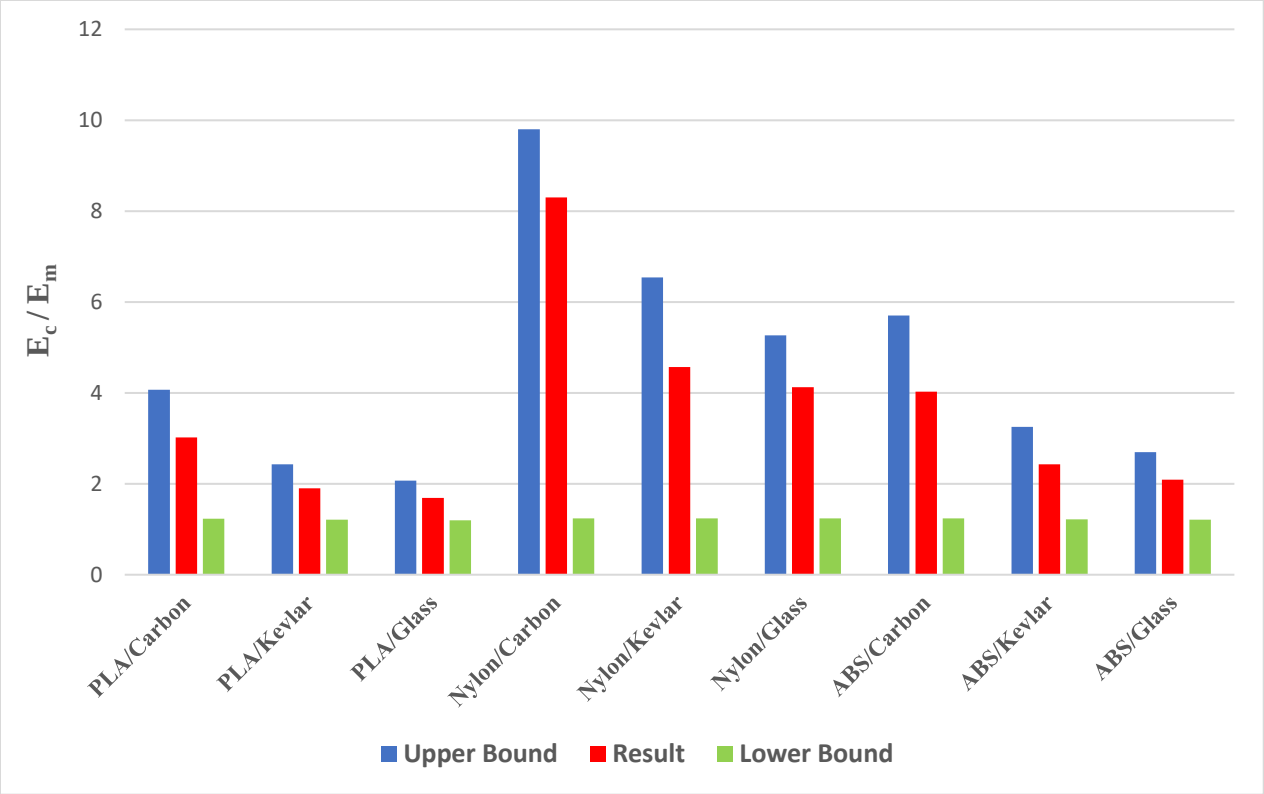

Figure 2. 5. The comparison of finite element results with the analytical models.

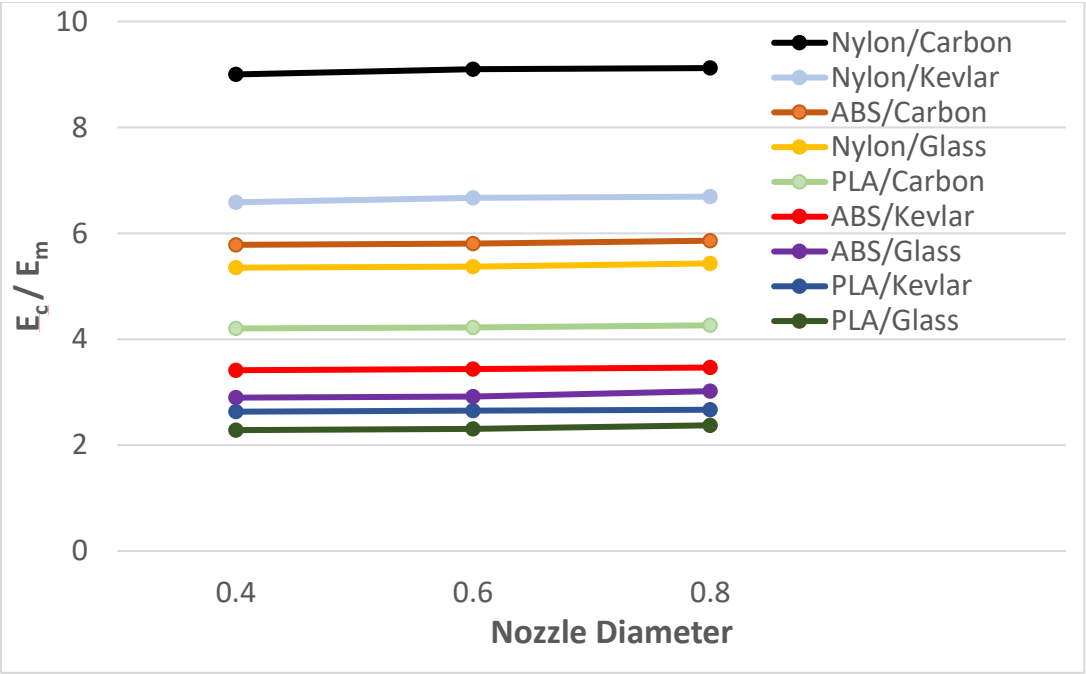

Figure 2. 6. Effect of nozzle diameter on the elastic modulus of continuous fiber composites

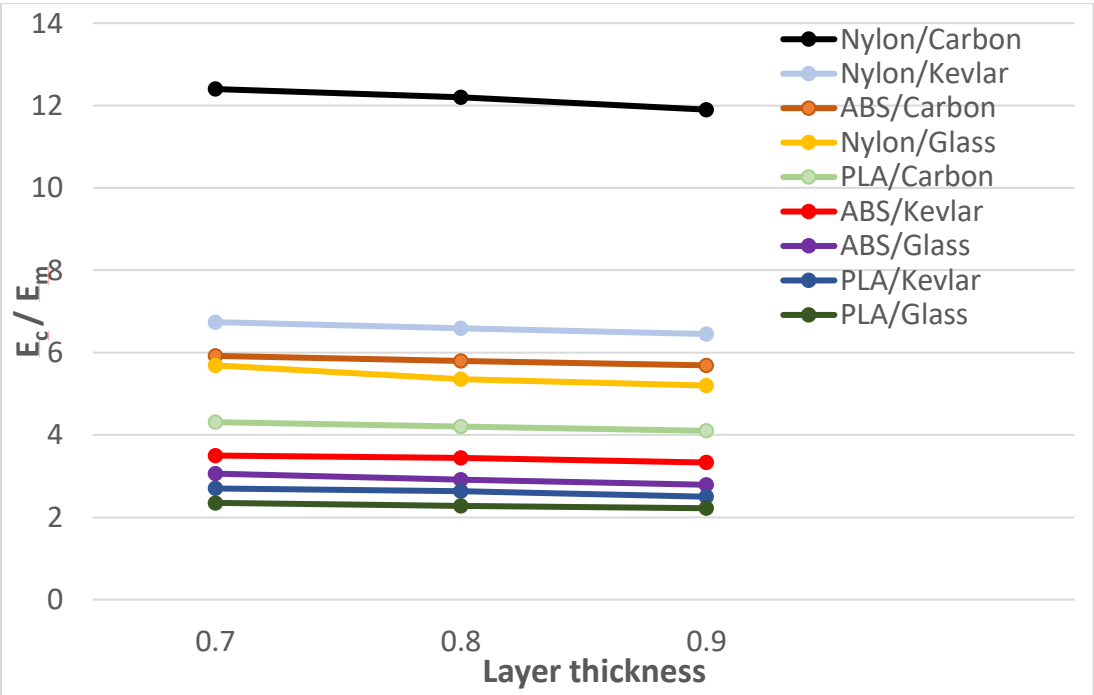

Figure 2. 7. Effect of layer thickness on the elastic modulus of continuous fiber composites

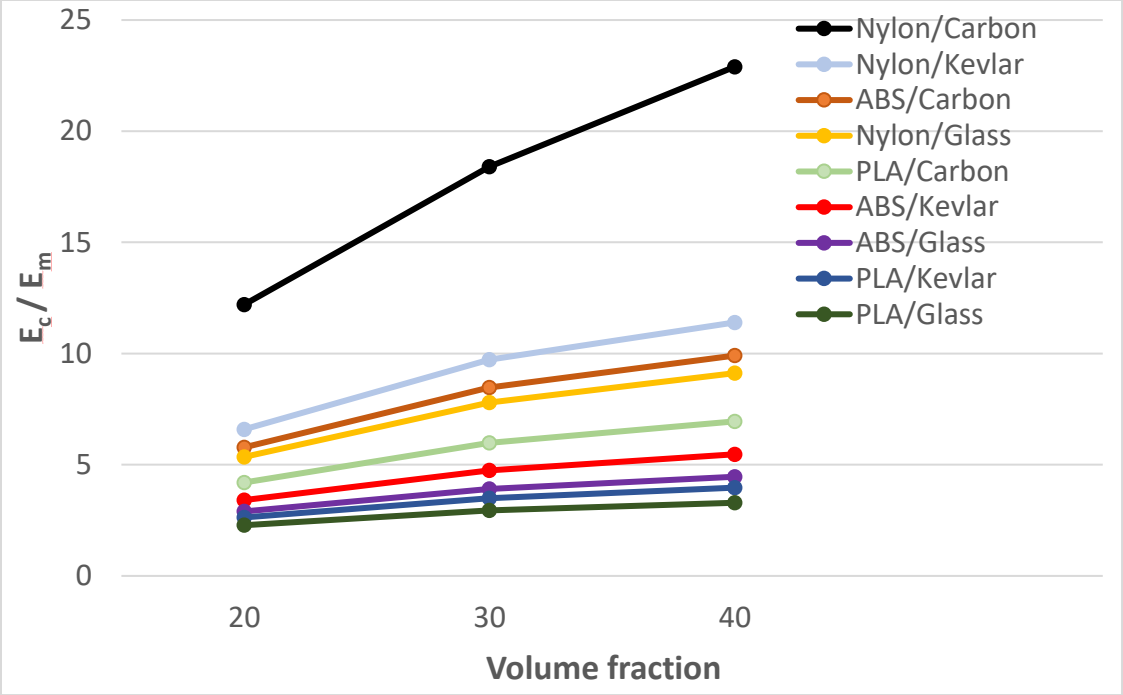

Figure 2. 8. Effect of volume fraction on the elastic modulus of continuous fiber composites

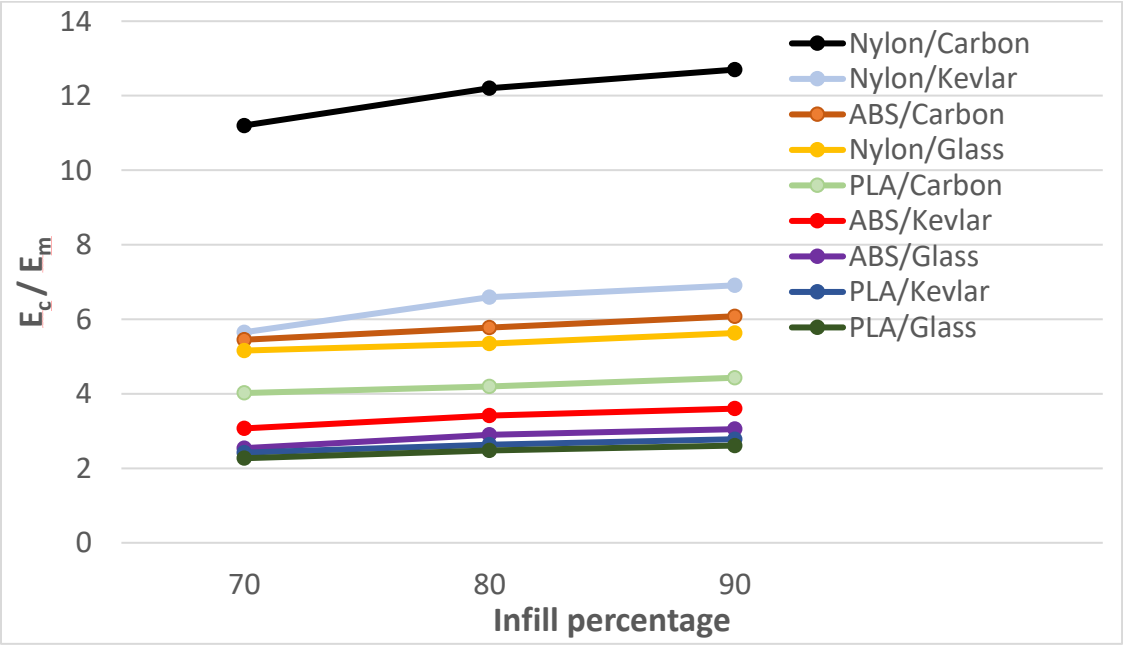

Figure 2. 9. Effect of infill percentage on the elastic modulus of continuous fiber composites

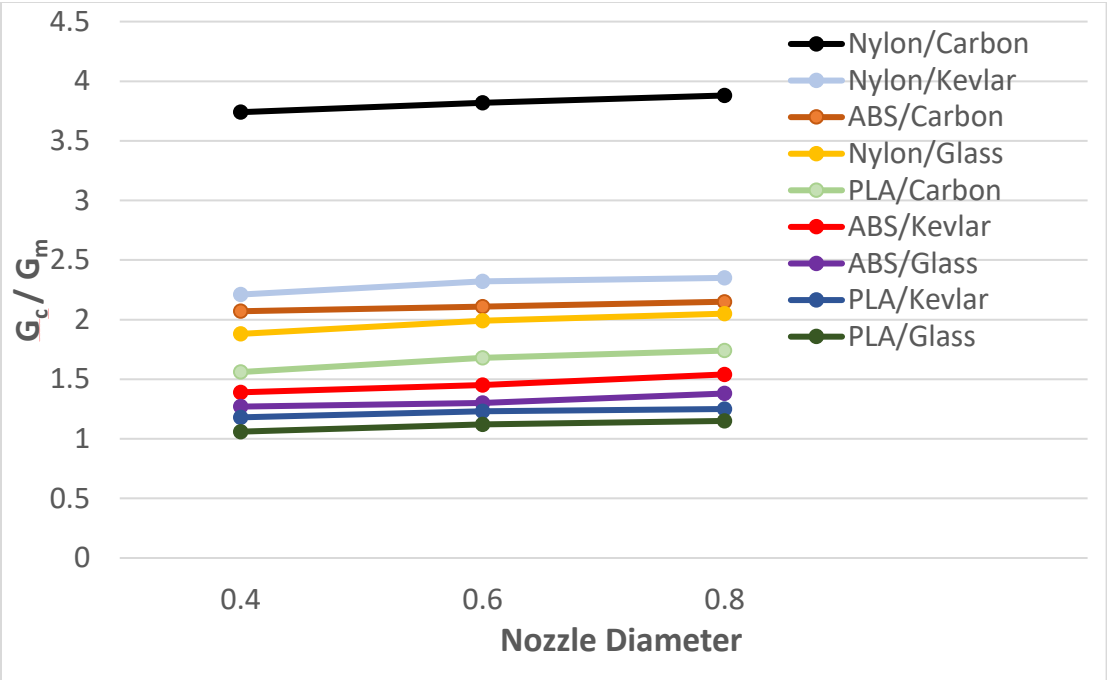

Figure 2. 10. Effect of nozzle diameter on the shear modulus of continuous fiber composites

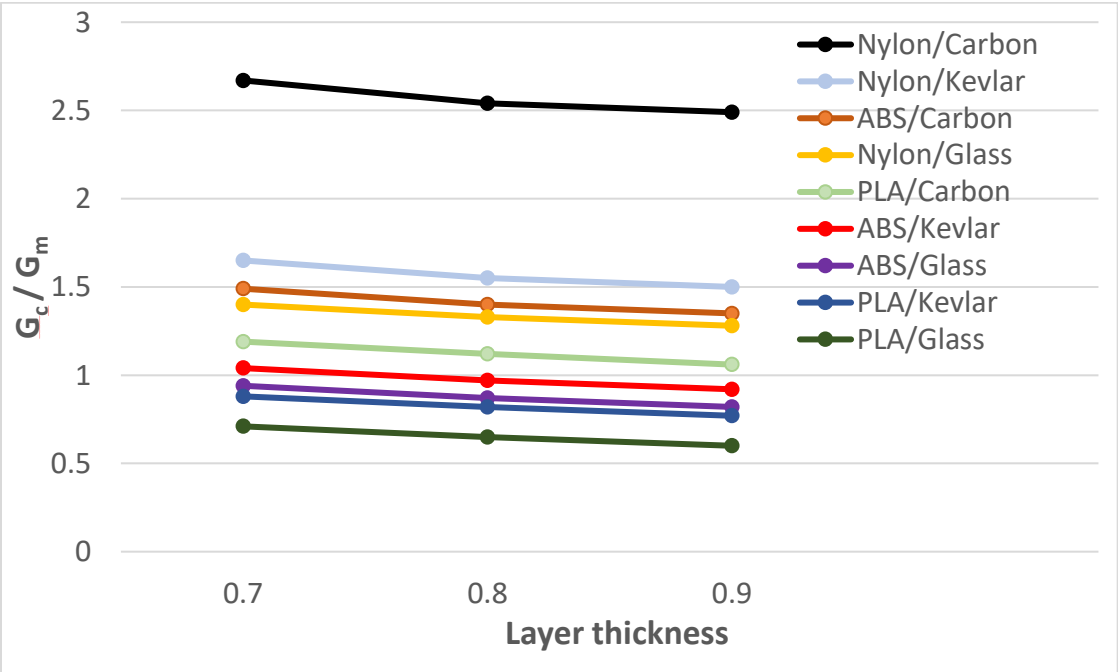

Figure 2. 11. Effect of layer thickness on the shear modulus of continuous fiber composites

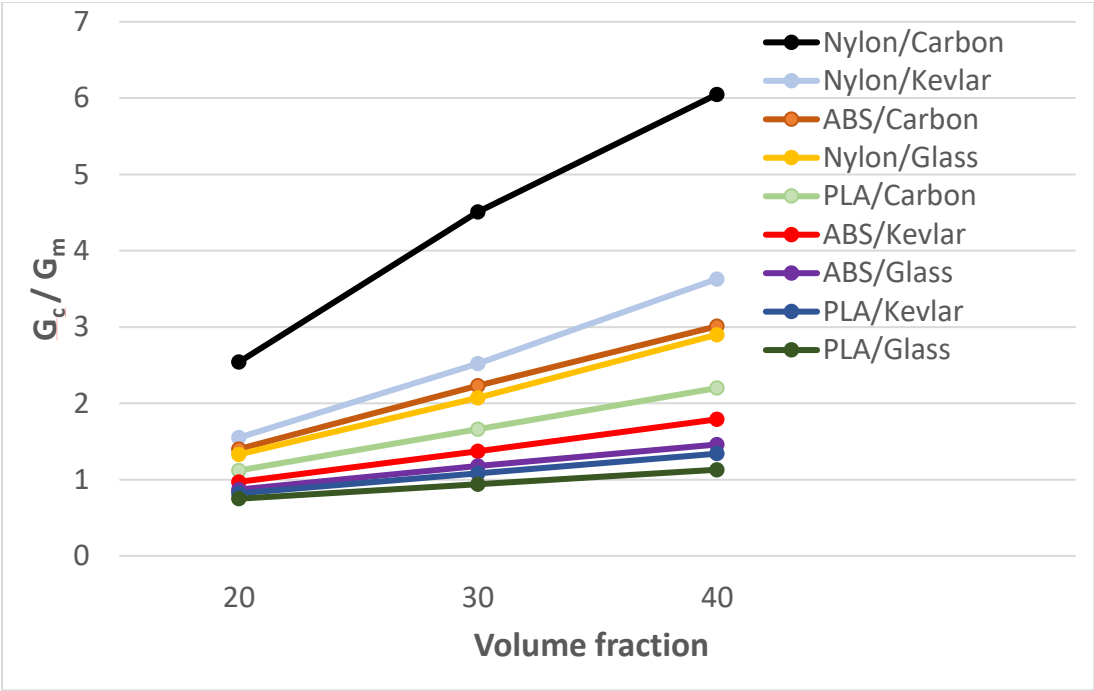

Figure 2. 12. Effect of volume fraction on the shear modulus of continuous fiber composites

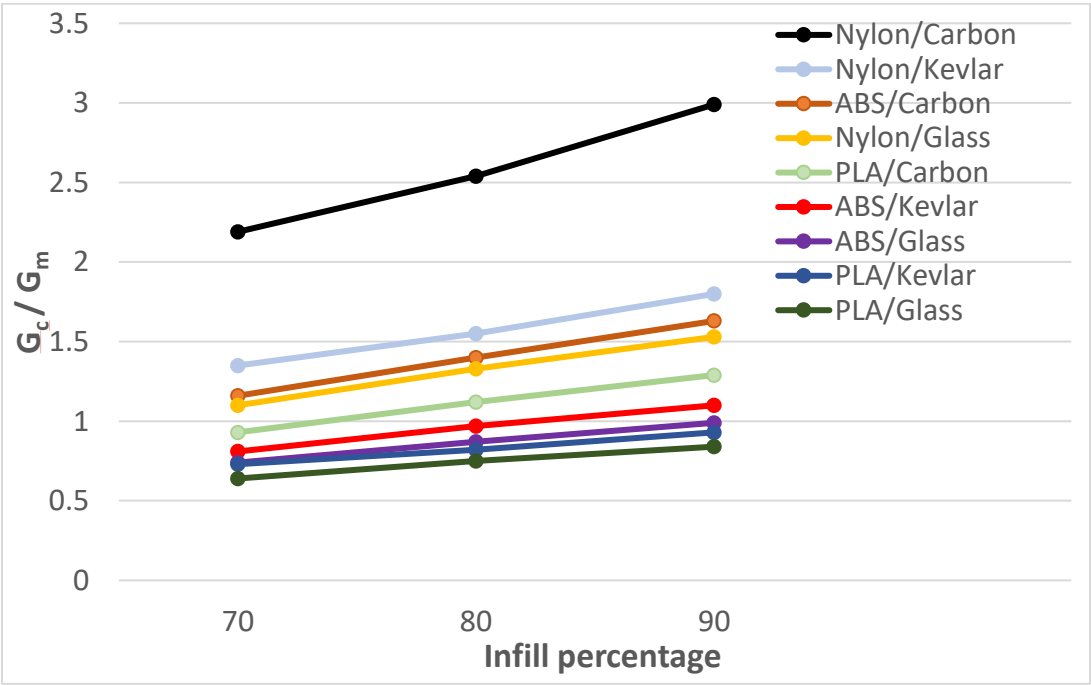

Figure 2. 13. Effect of infill percentage on the shear modulus of continuous fiber composites

The values of all elastic properties are negligibly affected by an increase in nozzle diameter. The elastic properties are decreasing with an increase in layer thickness. All the elastic properties increase with an increase in volume fraction and layer thickness. The elastic properties of carbon fibers are highest, followed by Kevlar and glass. The order of ratio of elastic modulus of composite with the pure thermoplastic is as follows: Nylon/Carbon > Nylon/Kevlar> ABS/Carbon > Nylon/Glass > PLA/Carbon > ABS/Kevlar > ABS/Glass > PLA/Kevlar > PLA/Glass.

2.6 Discussion

Following trends can be deduced from the results of the analysis.

- The 3D printed composite structures possess transversely isotropic properties since the values of E_1 and E_2, and G_{13} and G_{23} are similar.
- The elastic properties negligibly affected by an increase in nozzle diameter.
- The elastic properties decrease by an increase in the layer thickness except for E_3 which shows an increase in values.
- All the elastic properties increase with an increase in fiber volume fraction.
- The shear modulus and elastic modulus in all directions increase with an increase in infill percentage.

3. Continuous path planning for additive manufacturing of continuous fiber composites

In this chapter, a novel and robust continuous deposition path planning algorithm has been presented for printing of continuous fiber composites using co-axial FDM process. The algorithm is capable of generating printing instructions for any singly connected geometry without causing under-deposition or over-deposition. Raster filling pattern has been employed since the deposited continuous fiber composites are required to provide directional mechanical properties to the part. The algorithm is explained in the methodology section.

3.1. Methodology

In this section, the methodology for continuous path planning will be explained. Raster fill methodology is used to generate a continuous deposition path along the scanning direction. The algorithm is implemented to obtain printing instructions for complex geometries.

3.2.1. Raster filling methodology

In path planning for additive manufacturing, the part is filled layer by layer. The part is divided into layers along *z*-direction in a process called slicing so that each layer can be filled independently. The corner points of the box enclosing the part are required for slicing process, so a bounding box is created for the geometrical model and corner points of the box are obtained. The corner points are used to calculate the minimum *z* and maximum *z* values of the box. These *z* values referred to Z_{min} and Z_{max}, respectively. The values for the nozzle diameter *dia*, the overlap factor O_f, and interlayer penetration factor I_P are dependent upon user input. Set of planes $PL = \{pl_i\}_{i=0,1,..I}$ parallel to *xy*-plane, from Z_{min} to Z_{max}, is generated while satisfying the following equations.

$$pl_{i+1}(z) - pl_i(z) = LT \qquad \forall\, i \qquad (1)$$

$$LT = dia * (1 - I_P) \qquad (2)$$

Here LT represents the layer thickness which is the effective distance between the layers by taking into account the nozzle diameter *dia* and the interlayer penetration factor I_P, and $pl_i(z)$ presents

the *z*-value of pl_iin *xyz* coordinate system. The planes are intersected with the geometric model *GM* to produce a set of closed contour curves $CL = \{cl_{i,j}\}_{i=0,1,..I;j=0,1,...J}$

$$cl_{i,j} = GM \cap pl_i \qquad \forall\, i, j \qquad (3)$$

$$cl_{i,0} = oc_i \qquad \forall\, i \qquad (4)$$

Equation (3) provides the intersection of a set of planes *PL* with the geometric model G*M* to produce closed contour curves $CL = \{cl_{i,j}\}_{i=0,1,..I;j=0,1..J}$. Here $cl_{i,j}$ represents *jth* closed contour curve in *ith* layer. Equation (4) provides the assumption that the outer curves $OC = \{oc_i\}_{i=0,1,..I}$ enclose all the inner curves in *ith* layer such that $OC \subseteq CL$. The mathematical equation for closed contour curves $cl_{i,j}$ can be parametrically represented as:

$$cl_{i,j}(t) = \{x(t), y(t), z(t)\} \quad \forall\, t \in [a_{i,j}, b_{i,j}] \rightarrow \mathcal{R}^2$$

$$cl_{i,j}|_{t=a_{i,j}} = cl_{i,j}|_{t=b_{i,j}} \quad \forall\, i,j \qquad (5)$$

Here $cl_{i,j}(t)$ represents the parametric equation of *jth* closed contour curve in *ith* layer w.r.t parameter *t* in the range between $[a_{i,j}, b_{i,j}]$.

For each outer curve oc_i, a rectilinear bounding box is created with corner point set $CP=\{cp_{1,i}, cp_{2,i}, cp_{3,i}, cp_{4,i}\}$. Here, x_i^{min} and y_i^{min} represent the minimum extent of the outer curve oc_i. Whereas, x_i^{max} and y_i^{max} represent the maximum extent of the outer curve oc_i. The bounding box with the corner points is shown in Figure. 3.1(a). For raster scanning, a set of lines $IL = \{il_{i,k}\}_{i=0,1,..I;k=0,1..K}$ where $il_{i,k}$ represent the kth intersecting line in i^{th} layer, is generated along $\hat{y}$ unit vector by connecting set of points $P1 = \{p_{i,k}^1\}_{i=0,1,..I;k=0,1,..k}$ and $P2 = \{p_{i,k}^2\}_{i=0,1,..I,k=0,1,..k}$ by following equations.

$$il_{i,k} = \overline{p_{i,k}^1 p_{i,k}^2} \qquad \forall\, i,k \qquad (6)$$

$$p_{i,k}^1 = (xl_{i,k}, y_i^{min}, pl_i(z)) \qquad \forall\, i,k \qquad (7)$$

$$p_{i,k}^2 = (xl_{ik}, y_i^{max}, pl_i(z)) \qquad \forall\, i,k \qquad (8)$$

Where $XL = \{xl_{i,k}\}_{i=0,1,..I;\, k=0,1,..k}$ is an arithmetic series such that

$$xl_{i,0} = x_i^{min} \qquad \forall\, i \qquad (9)$$

$$xl_{i,K} = x_i^{max} \qquad \forall\, i \qquad (10)$$

$$xl_{i,k+1} - xl_{i,k} = D \qquad \forall\, i,k \qquad (11)$$

$$D = dia * (1 - O_f) \qquad (12)$$

D represents the effective distance between the lines $il_{i,k}$ by taking into account the nozzle diameter *dia* and overlap factor O_f. While scanning, they are intersected by the curves $cl_{i,j}$ in the ith layer to create intersection points $IP = \{ip_{i,k,l}\}_{i=0,1,..I;\ k=0,1,..k\ ;l=0,1,..L}$ where $ip_{i,k,l}$ is the lth intersection point which is obtained when the kth line intersects curves $cl_{i,j}$ in the ith layer. These intersection points are used to produce the set of deposition points $DP = \{dp_p\}_{p=0,1,..P}$ in a zig-zag manner, where dp_p is the pth deposition point. The deposition of points by the intersection of lines is shown in Figure. 3.1(b).

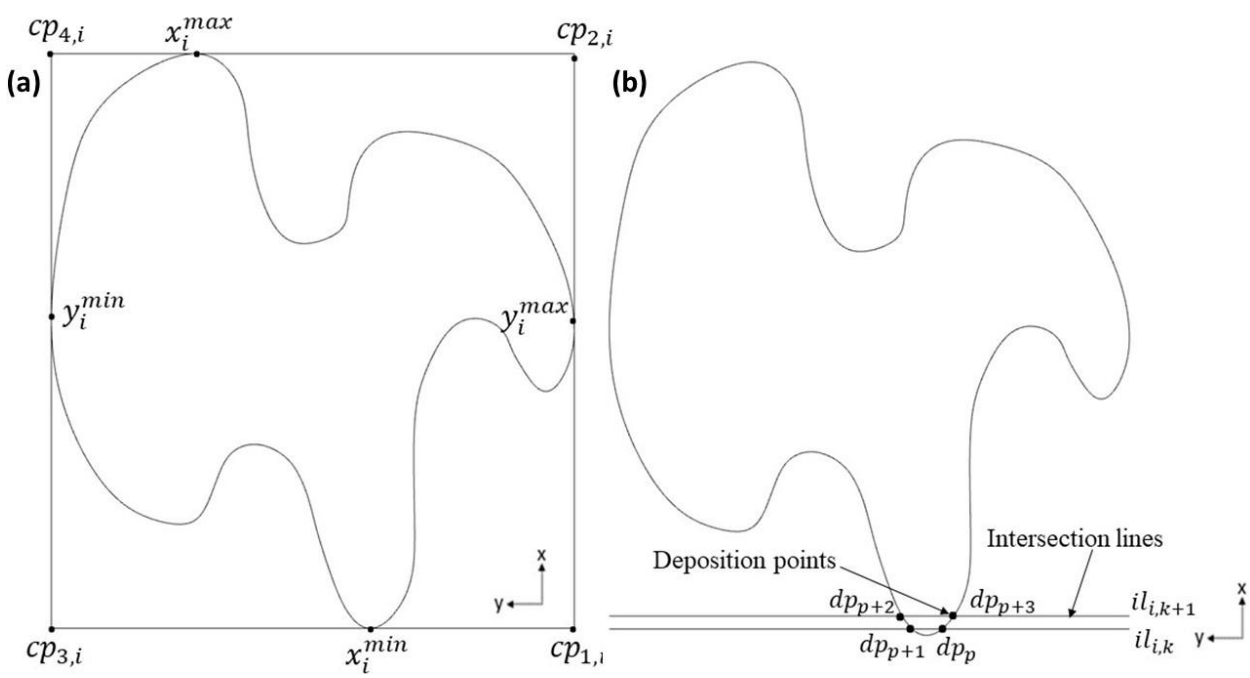

Figure 3. 1. (a) Bounding box with corner points of the curve (b) Deposition of points by the intersection of lines

The algorithm for the generation of deposition points is given below.

$EO \leftarrow 0$ /* even odd check variable

For all $il_{i,k}$ in IL

$ip_{i,k,l} = cl_{i,j} \cap il_{i,k} \quad \forall\ i,j,k,l$ /* intersection of line with curves

Sort $ip_{i,k,l}$ such that $ip_{i,k,l+1}(y) > ip_{i,k,l}(y) \quad \forall\ i,k,l$ /* Points are sorted in increasing *y*-coordinate values where $ip_{i,k,l}(y)$ is the *y*-coordinate value of point $ip_{i,k,l}$ */

If $EO\ mod\ 2 = 0$ **Then**

$DP \leftarrow DP \cup ip_{i,k,0}$

$DP \leftarrow DP \cup ip_{i,k,1}$

Else

$DP \leftarrow DP \cup ip_{i,k,1}$

$DP \leftarrow DP \cup ip_{i,k,0}$

End If

$EO \leftarrow EO + 1$

End Loop

The lines are referred as either "even" line or "odd" line depending upon the value of *k*. The intersection points $Ip_{i,k,l}$ are ordered in a way that a zig-zag deposition path is generated for raster filling.

3.2.4. Determination of extremum points along the scanning direction

The determination of maximum and minimum points is very important information to avoid having unfilled regions and deposition outside the part while filling continuously. The maximum and minimum points are calculated using the derivative of the curve along the scanning direction. While scanning along the *x*-direction, for the parametric curves $cl_{i,j}(t) = \{x(t), y(t), z(t)\}$, the extremum points lie on $cl_{i,j}(t)$ at parameter $t^{/}$ when following condition is satisfied:

$$\frac{dx(t^{/})}{dy(t^{/})} = 0 \qquad \forall\ t^{/} \in [a_{i,j}, b_{i,j}] \qquad (13)$$

The curve $cl_{i,j}(t^{/})$ contains a maximum point at $t^{/}$ if $\frac{d^2x(t^{/})}{dy^2(t^{/})} < 0$, and $cl_{i,j}(t^{/})$ contains a minimum point at $t^{/}$ if $\frac{d^2x(t^{/})}{dy^2(t^{/})} > 0$. For each curve $cl_{i,j}$ the maximum points are stored as $MCX = \{mxc_{i,j,m}\}_{i=0,1,..I;\ j=0,1,..J\ ;\ m=0,1,..M}$ where $mxc_{i,j,m}$ represents the mth maximum point on the jth curve in the ith layer. Similarly, the minimum points are stored as $MNC = \{mnc_{i,j,n}\}_{i=0,1,..I;\ j=0,1,..J\ ;\ n=0,1,..N}$ where $mnc_{i,j,n}$ represents the nth maximum point on the jth curve in the ith layer. A curve containing the maximum and minimum points is shown in Figure. 3.2.

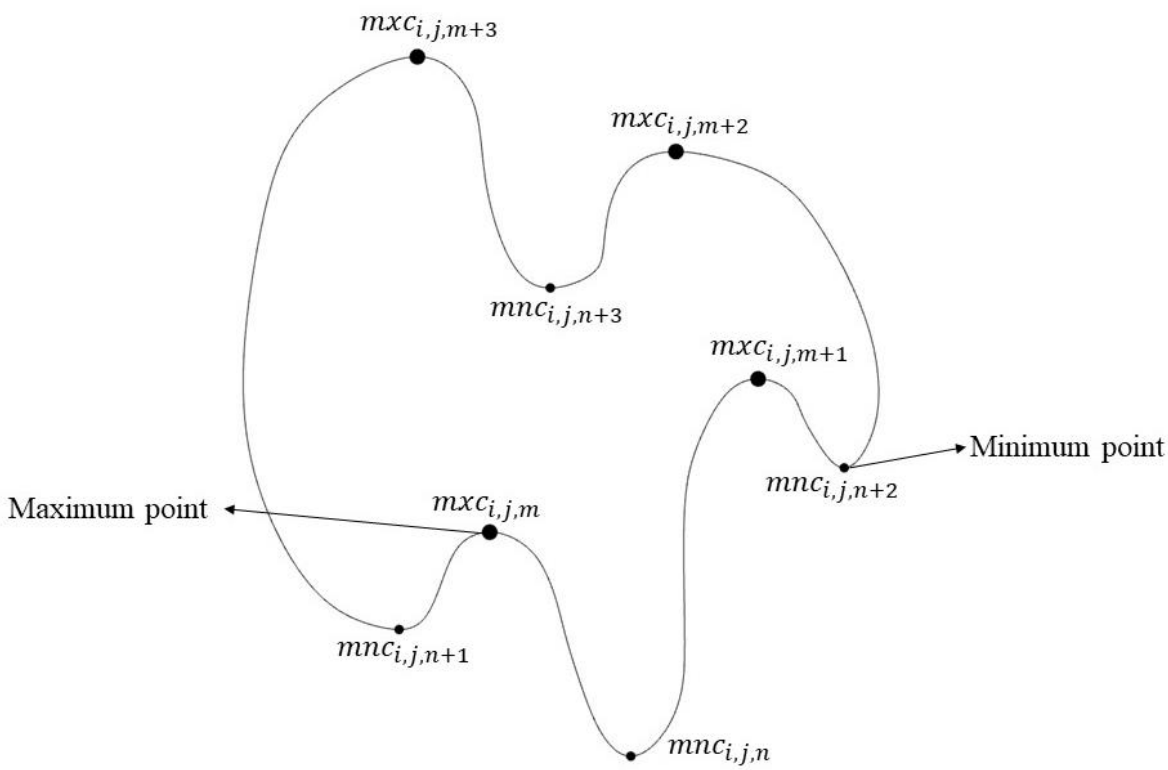

Figure 3. 2. The curve containing the maximum and minimum points

While scanning along *y*-direction in the next layer, the extremum points are calculated in the same manner. The only difference is that the derivative of $y(t)$ is taken with respect to $x(t)$.

3.2.5. Deposition path generation

While scanning along *x*-direction, the deposition path points dp_p and dp_{p+1} on the same intersection line $il_{i,k}$ are always $ip_{i,k,0}$ and $ip_{i,k,1}$ (the lowest *y*-value points) of the array of intersections points $ip_{i,k,l}$ obtained from intersection of line $il_{i,k}$with all the curves $cl_{i,j}$ in the ith layer so the deposition path points *DP* remain on the lower *y* side of the geometry. When even the

intersection line $il_{i,k} \forall\ k$ mod *2=0* passes a maximum point $mxc_{i,j,m}$, the maximum point *max* is obtained and the curve containing the maximum point *max* in the set of curves *CL* is obtained and denoted by *CM* such that $CM \in CL$. The parametric value of *max* on *CM* is denoted as P_m. All the minimum points on the curve *CM* with parametric value greater than P_m are stored in $PRG = \{prg_r\}_{r=0,1,..R}$ such that $prg_r > P_m$. Similarly, all the minimum points on the curve *CM* with a parametric value smaller than P_m are stored in $PRS = \{prs_s\}_{s=0,1,..S}$ such that $prs_s < P_m$. The sets PRG and PRS are sorted in ascending order. Using these two sets, the next minimum point *min* on *CM* along *y*-axis is obtained. This procedure is shown in Figure. 3.3. The deposition on the curve takes place from *max* point to that *min* point, such that the *x* distance between the points is equal to *D*, and then the raster scanning takes place again from *min* point to *max* point as explained in section 3.2.1. Similar variables are used in the algorithm with index "/". The deposition of points is shown in the blue section in Figure. 3.5.

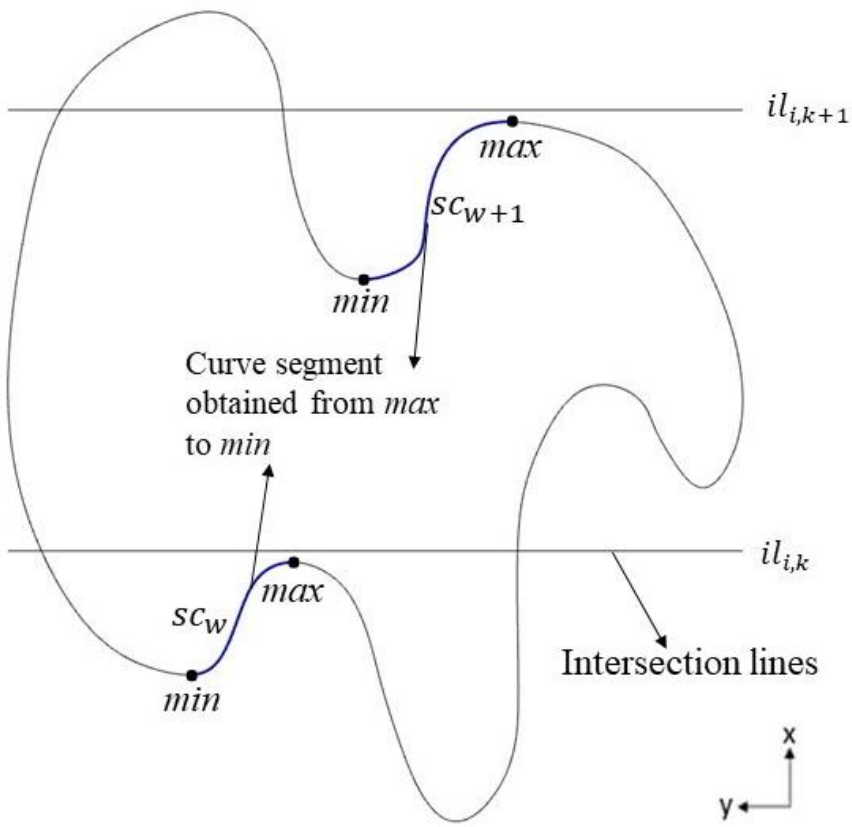

Figure 3. 3. Obtaining the curve segment sc_w for *ReturnPoints* function

The detailed algorithm is given below.

$SC = \{sc_w\}_{w=0,1,..W}$ /* Set containing all the curve segments

Function *ReturnPoints(max, SC,* y_i^{min}, y_i^{max}, *CL, D, DP)*

EO ← *0* //Initializing the even odd check variable

If Size of *PRG* > *0* **Then**

min1 ← prg_0

Else

min1 ← prs_0

End If

If Size of *PRS* > *0* **Then**

min2 ← prs_S

Else

min2 ← prg_R

End If

sc1← Curve segment from *max* to *min1*

sc2← Curve segment from *max* to *min2*

If *min1(y)* > *min2(y)* **Then**

sc′← *sc1*

min← *min1*

Else

sc′← *sc2*

min← *min2*

End If

SC ← *SC* ∪ *sc′*

SCP=$\{scp_q | scp_0 = max \wedge scp_Q = min \wedge scp_{q+1}(x) - scp_q(x) = D\}_{q=0,1,..Q} \quad \forall q$ /* Divide *sc′* into set of points *SCP* such that the end points of the segment are equal to *max* and *min* and *x*-distance between the points is equal to *D* */

DP ← *DP* ∪ *SCP*

Reverse the elements of *SCP*

$il^{/}_{i,k^{/}} = \overline{p^{1}_{i,k^{/}} p^{2}_{i,k^{/}}}$ $\forall i, k^{/}$

$p^{1}_{i,k^{/}} = (scp_q(x)\ , scp_q(y)\ , scp_q(z))$ $\forall i, k^{/}, q$

$p^{2}_{i,k^{/}} = (scp_q(x), y_i^{max}, scp_q(z))$ $\forall i, k^{/}, q$

For all $il^{/}_{i,k^{/}}$ in $IL^{/}$

$ip^{/}_{i,k^{/},l^{/}} = sc^{/} \cap il^{/}_{i,k^{/}}$ $\forall i, k^{/}, l^{/}$

Sort $ip^{/}_{i,k^{/},l^{/}}$ such that $ip^{/}_{i,k^{/},l^{/}+1}(y) > ip^{/}_{i,k^{/},l^{/}}(y)$ $\forall i, k^{/}, l^{/}$

If *EO* mod *2=0* **Then**

$DP \leftarrow DP \cup ip^{/}_{i,k^{/},0}$

$DP \leftarrow DP \cup ip^{/}_{i,k^{/},1}$

Else

$DP \leftarrow DP \cup ip^{/}_{i,k^{/},1}$

$DP \leftarrow DP \cup ip^{/}_{i,k^{/},0}$

End If

$EO \leftarrow EO+1$

End For

End Function

The deposition of points are shown in the blue section in Figure. 3.5**.**

3.2.6. Avoiding deposition outside the part

In concave shapes, the deposition path points dp_p and dp_{p+1}, on the consecutive lines $il_{i,k}$and $il_{i,k+1}$, can be far away from each other in terms of distance along *y* that it can lead to a situation in which there is deposition outside of the curve while connecting the path between deposition path points.

To check whether this situation is happening or not, a function *FollowCurve* is called that takes the curve segment sc_w between the deposition path points dp_p and dp_{p+1}on every every two consecutive lines $il_{i,k}$and $il_{i,k+1}$, and checks whether a maximum point $mxc_{i,j,m}$exists on the curve segment or not. If the condition is satisfied, the deposition path points are added on the curve segment such that the *x*-distance between the points is equal to *D*. This procedure is shown in Figure. 3.4. and the deposition of points along the curve segment is shown in the red section in Figure. 3.5.

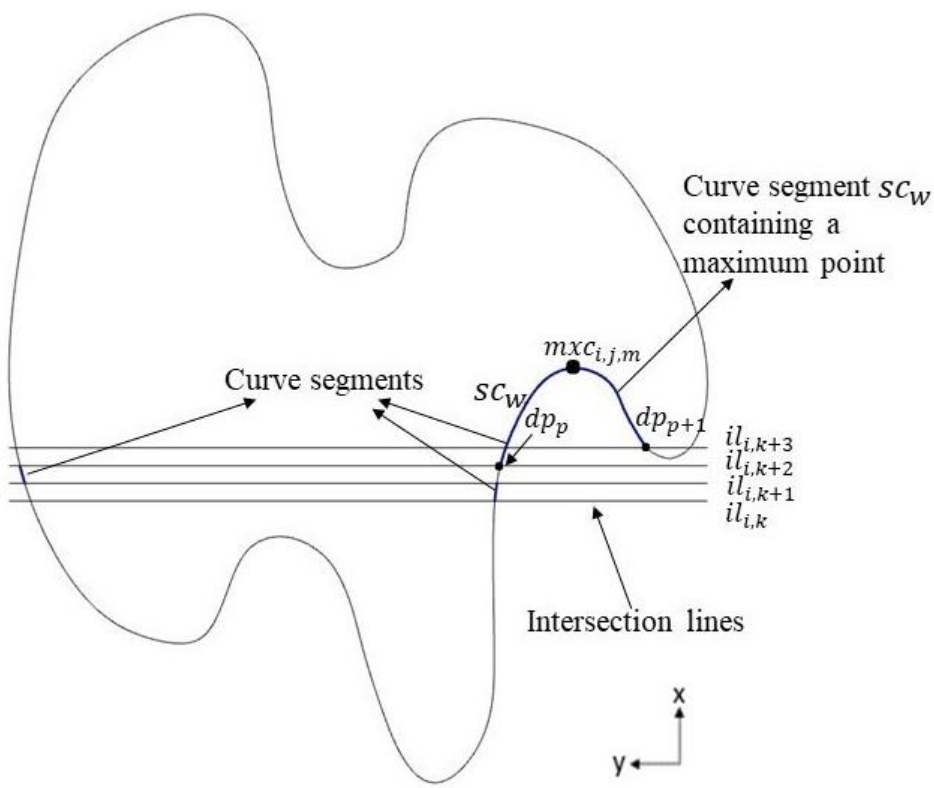

Figure 3. 4. Obtaining the curve segment sc_w for deposition along the curve

The pseudo code for the algorithm is given below.

Function *FollowCurve(*dp_p*,* dp_{p+1}*, SC, MXC, MNC, CL, D, DP)*

$sc^{/}$ ← curve segment from dp_{p+1} to dp_p

If $dp_{p+1}(x) - dp_p(x) = D$ **Then** /* Condition that the points are on the consecutive intersection lines, not on the same line. $dp_p(x)$ represents *x*-value of dp_p */

For each $mxc_{i,j,m}$ in *MXC*

If $mxc_{i,j,m}$lies on $sc^{/}$ **Then**

$SC \leftarrow SC \cup sc^{/}$

$SCP=\{scp_q | scp_0 = dp_{p-1} \wedge scp_Q = dp_p \wedge scp_{q+1}(x) - scp_q(x) = D\}_{q=0,1,..Q}$ /* Divide $sc^{/}$ into set of points *SCP* such that the end points of the segment are equal to dp_p and dp_{p-1} and *x*-distance between the points is equal to *D* */

$MNC \leftarrow MNC \cup dp_{p-1}$

$DP \leftarrow DP \cup SCP$

End If

End For

End If

End Function

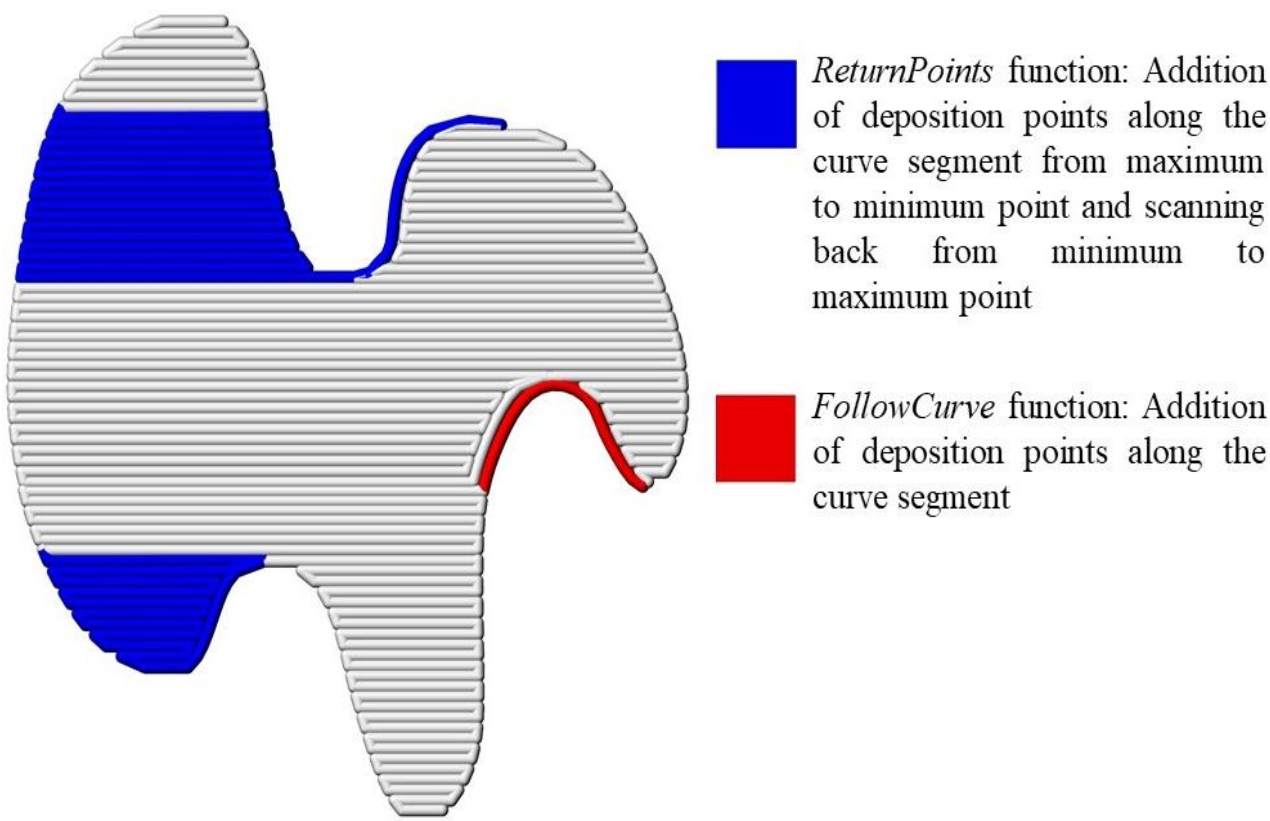

Figure 3. 5. Continuous filling of a complex concave geometry

3.2.7. Avoiding the over-deposition

There are certain regions in the part where there can be over deposition. To avoid that situation, after all the deposition path points are obtained, each point is checked whether it lies on any of the curve segment sc_w or not. If it lies on a curve segment then, depending on whether the curve segment is a part of the outer or inner curve, the deposition path point is offset along the normal direction to that curve. If the point dp_p lies on the outer curve it is offset inwards, while if it lies one of the inner curves, it is offset outwards along the normal direction to the curve.

The point is offset along the unit normal direction $\vec{N}$ by distance *D* can be found with the following equation:

$$dp_p = dp_p \pm N * D \qquad (14)$$

Where $\vec{N}$ is unit normal vector on contour curve $cl_{i,j}$ at point dp_p in outward direction.

The algorithm is given in pseudocode form below.

Function *OverdepositionCheck (DP, SC, CL, D)*

 For each dp_p in *DP*

  For each sc_w in *SC*

   If dp_p lies on sc_w **Then**

    If dp_p lies on oc_i **Then**

     $dp_p \leftarrow dp_p + N * D$

    Else

     $dp_p \leftarrow dp_p - N * D$

    End If

   End If

  End For

 End For

End Function

The overall algorithm for continuous path planning is explained in sequence in Figure 3.6.

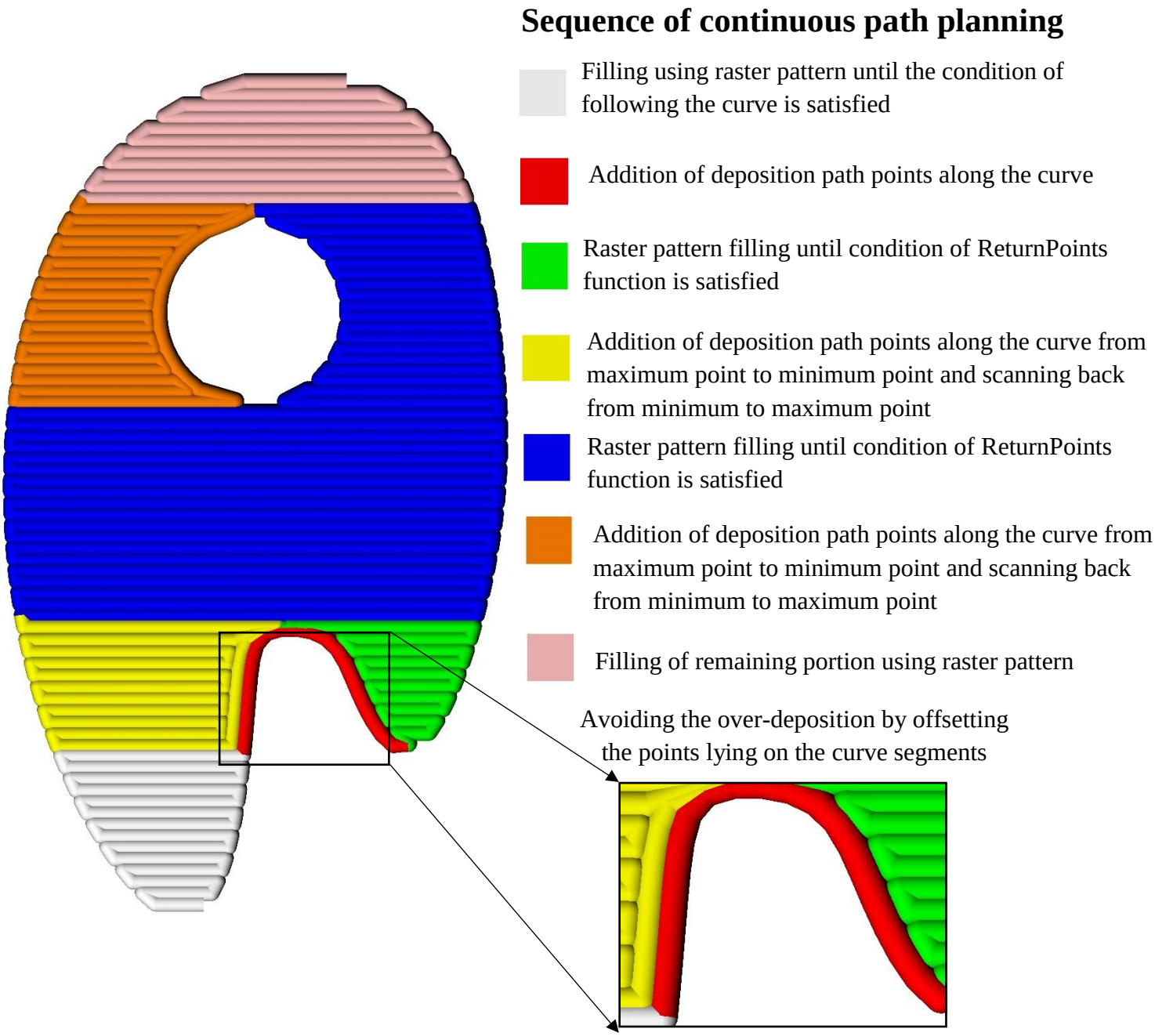

Figure 3. 6. Explanation of continuous path planning algorithm on a complex geometry

3.2.8. Filling of boundary and moving to the next layer

After the filling inside the first layer is complete, the outer boundary is plotted. To move to the second layer while printing continuously, deposition path is generated such that the printhead moves upwards along *z*-direction by a distance equal to *LT*. Then *FollowCurve* function deposits along the internal offset curve of the second layer by following the curve until it reaches the start point of deposition in the second layer. The scanning takes place along *y*-direction in the second layer and then the outer boundary is plotted. The scanning process takes place using the same algorithm in the second layer but along the *y*-direction. After the second layer is deposited, scanning takes place on the third layer along the *x*-direction. This process continues until the last layer is filled. The process is explained in Figure 3.7.

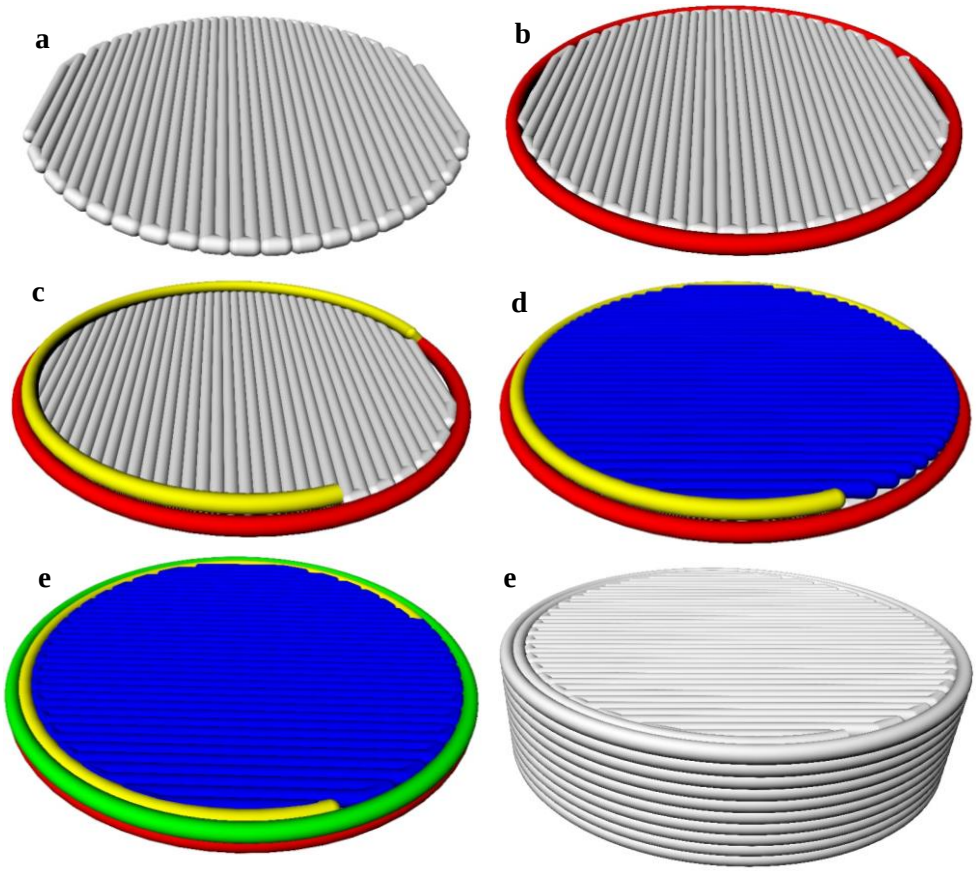

Figure 3.7. Filling of a complete 3D model (a)Filling inside internal offset curve in first layer (b) Plotting the boundary of first layer (c) Filling along the internal offset curve in the second layer (d) Raster pattern scanning along y-direction in internal offset curve in second layer (e)Filling of boundary of second layer (f) Filling of a complete 3D model

3.3. Results

3.3.1. Comparison with commercial software

The algorithm has been implemented on complex shape geometries. Figure. 3.8. shows an illustration of the deposition process on a complex concave shape geometry. A layer with a complex geometry is deposited in Figure 3.6. The path generated by using the developed algorithm is compared with that of Eiger, which is path planning software from Markforged 3D printer, a commercial printer that is capable of printing continuous fiber composites.

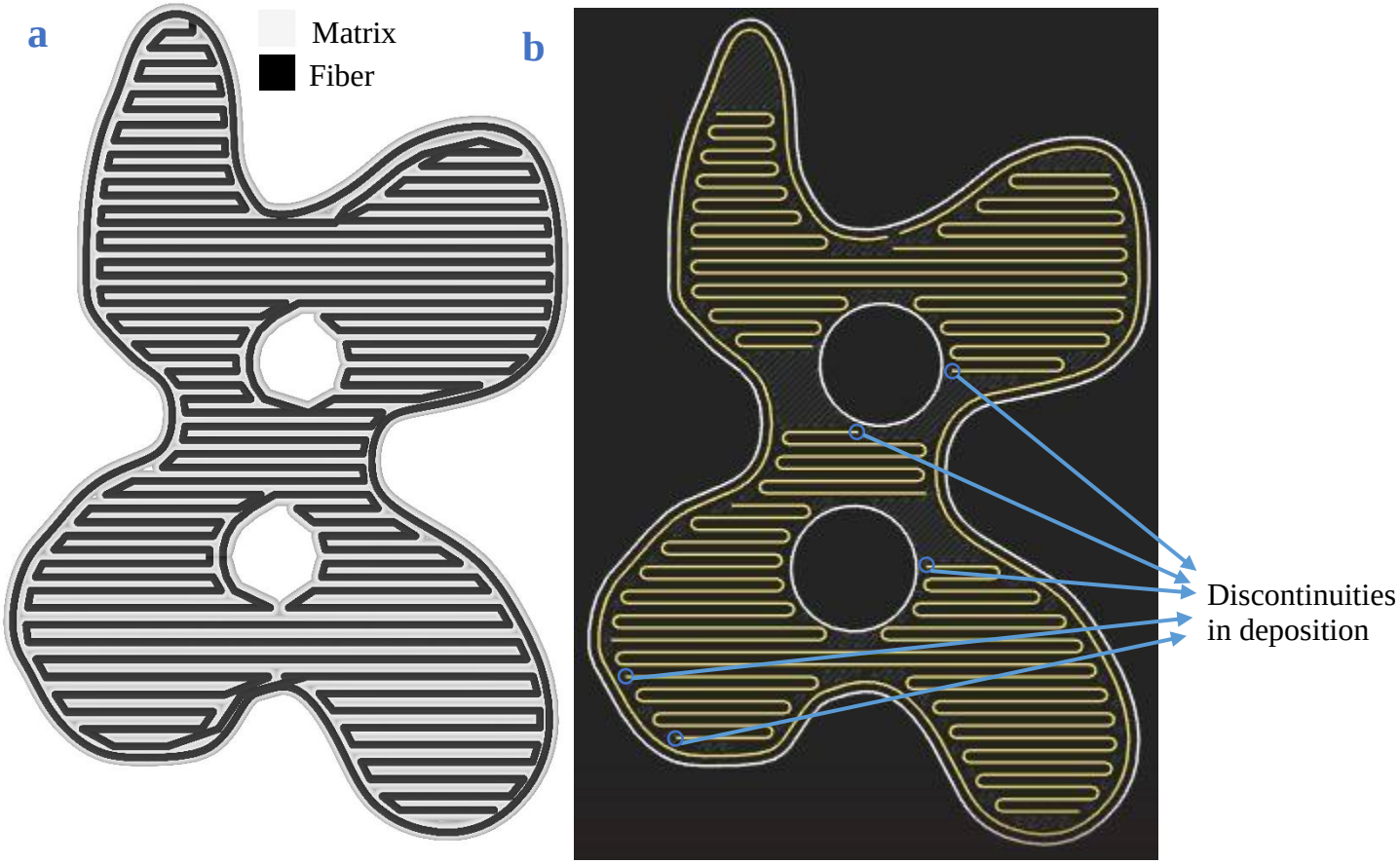

Figure 3. 8. Deposition path planning of a complex concave shape geometry (a) Using continuous path planning algorithm (b) using commercial software

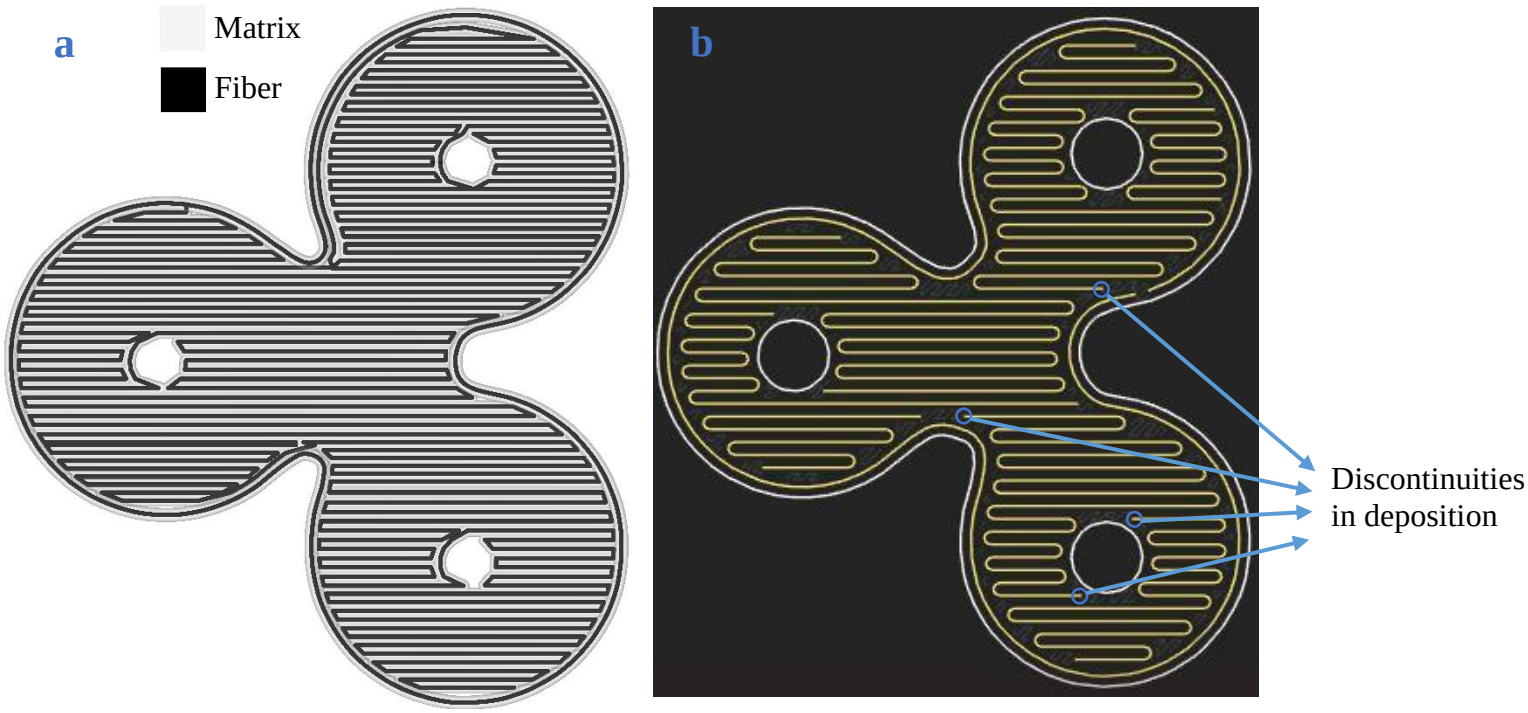

Figure 3. 9. Deposition path planning of a fidget spinner (a) Using continuous path planning algorithm (b) using commercial software

It is evident from the figures that there are several discontinuities and unfilled regions in the path generated by the commercial software. Whereas the path generated using the developed algorithm is continuous, and the whole layer is filled without any over-deposition. Therefore, it can be successfully applied for 3D printing of CFRTP composites.

3.3.2. Implementation on a 3D printer

The printing instructions generated from the algorithms were implemented on the Ultimaker 2 3D printer to test the applicability of the algorithm. Ultimaker was chosen because it is an open source printer and the printing instructions can be easily applied. The results are shown in Figure 3.10.

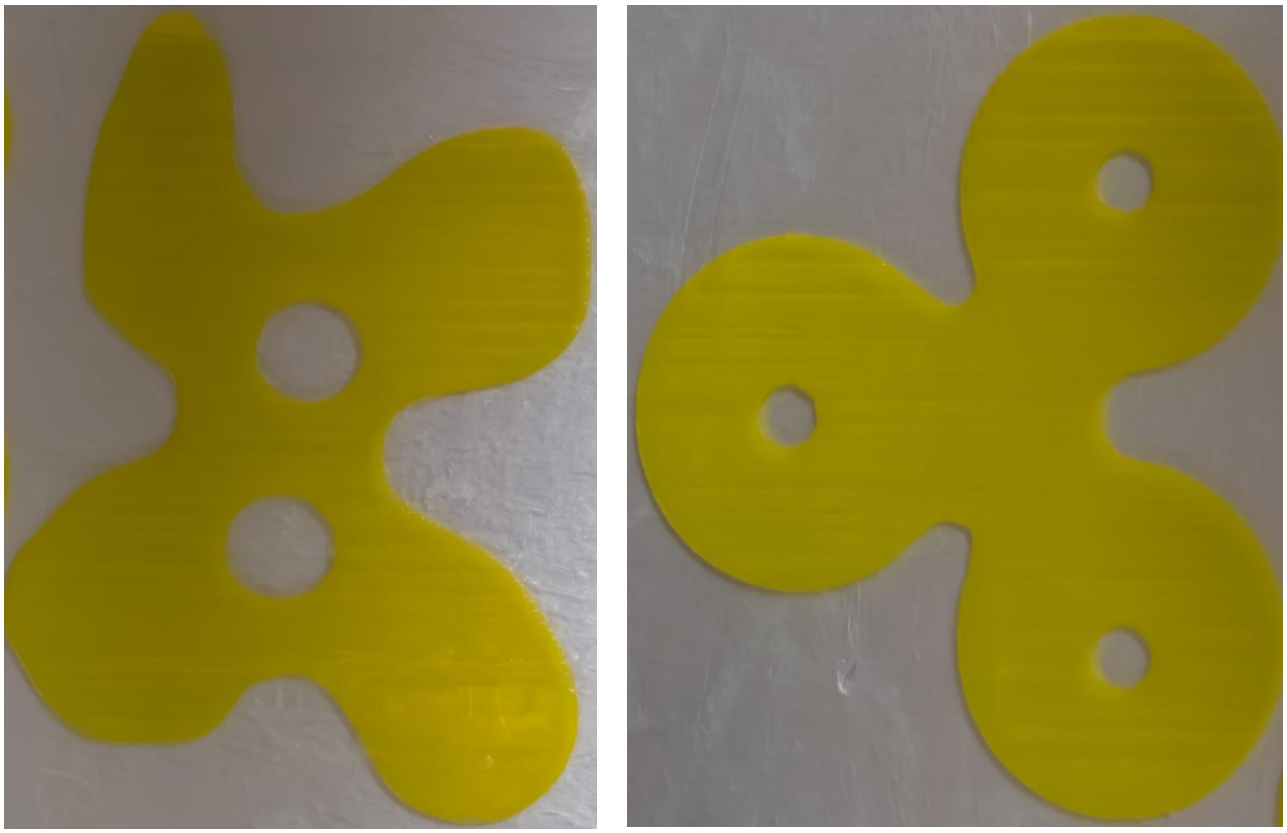

Figure 3.10. Implementation of the developed algorithm on a commercial printer (a) Complex concave geometry (b) Fidget spinner

4. Conclusion and future work

The main objective of this thesis is for modeling and path planning of continuous fiber reinforced thermoplastic composite structures. Additive manufacturing of continuous fiber composites using coaxial extrusion process can be a very effective solution to improve the mechanical properties of the parts produced using fused deposition modeling process. Since the current studies for evaluation of the mechanical properties of additively manufactured CFRTP composites are based on experimental studies, there is a very limited work available for determining and optimizing the process parameters. Therefore, a detailed analysis is required to study the effect of process parameters such as nozzle diameter, layer thickness, infill percentage and volume fraction on effective elastic properties of CFRTP composites. Moreover, to fully utilize these parameters to

produce a complex shape parts, a continuous path planning algorithm is required that can produce a deposition path for any singly connected curve shaped object.

A finite element analysis of additively manufactured continuous fiber composites has been developed. The geometries were modeled, and finite element analysis was used to study the effect of different parameters on mechanical properties of 3D printed continuous fiber composites with different matrix and fiber combinations. It was observed that the additively manufactured composite structures possess transversely isotropic properties. The obtained results showed that elastic properties increased with an increase in nozzle diameter, volume fraction and infill percentage, and decreased with an increase in layer thickness.

A continuous deposition path planning algorithm has also been developed for printing of CFRTP composites. The use of continuous fibers as reinforcement makes it very challenging to print complex shape parts because the use of continuous fiber as a reinforcement requires continuous deposition of material throughout the printing process. To address this issue, a novel path planning algorithm has been developed that can generate a continuous deposition path to print complex shape parts without any under-deposition or over-deposition. This study can provide an effective solution to extend the application of the continuous coaxial fibers composite printing technique to the parts with industrial applications.

As a future work, a screw based mechanism can be designed and developed for 3D printing of CFRTP composites. It would allow the continuous input of thermoplastic pallets and, therefore, parts with large dimensions can be printed. In addition, a topology optimization based algorithm can be developed to control the number of layers containing fibers to produce optimized lightweight parts depending upon specific load applications.

5. References

[1] Y. Huang, M. C. Leu, J. Mazumder, and A. Donmez, "Additive Manufacturing: Current State, Future Potential, Gaps and Needs, and Recommendations," *J. Manuf. Sci. Eng.*, vol. 137, no. 1, p. 014001, 2015.

[2] H. Bikas, P. Stavropoulos, and G. Chryssolouris, "Additive manufacturing methods and modeling approaches: A critical review," *Int. J. Adv. Manuf. Technol.*, vol. 83, no. 1–4, pp. 389–405, 2016.

[3] B. Berman, "3-D printing: The new industrial revolution," *Bus. Horiz.*, vol. 55, no. 2, pp. 155–162, Mar. 2012.

[4] A. K. Sood, R. K. Ohdar, and S. S. Mahapatra, "Parametric appraisal of mechanical property of fused deposition modeling processed parts," *Mater. Des.*, vol. 31, no. 1, pp. 287–295, 2010.

[5] W. Gao, Y. Zhang, D. Ramanujan, K. Ramani, Y. Chen, C. B. Williams, C. C. L. Wang, Y. C. Shin, S. Zhang, and P. D. Zavattieri, "The status, challenges, and future of additive manufacturing in engineering," *CAD Comput. Aided Des.*, vol. 69, pp. 65–89, 2015.

[6] B. N. Turner and S. A. Gold, "A review of melt extrusion additive manufacturing processes: II. Materials, dimensional accuracy, and surface roughness," *Rapid Prototyp. J.*, vol. 21, no. 3, pp. 250–261, 2015.

[7] D. Roberson, C. M. Shemelya, E. MacDonald, and R. Wicker, "Expanding the applicability of FDM-type technologies through materials development," *Rapid Prototyp. J.*, vol. 21, no. 2, pp. 137–143, 2015.

[8] K. S. Boparai, R. Singh, and H. Singh, "Development of rapid tooling using fused deposition modeling: a review," *Rapid Prototyp. J.*, vol. 22, no. 2, pp. 281–299, 2016.

[9] I. Durgun and R. Ertan, "Experimental investigation of FDM process for improvement of mechanical properties and production cost," *Rapid Prototyp. J.*, vol. 20, no. 3, pp. 228–235, 2014.

[10] S. Ford and M. Despeisse, “Additive manufacturing and sustainability: an exploratory study of the advantages and challenges,” *J. Clean. Prod.*, vol. 137, pp. 1573–1587, 2016.

[11] C. S. Lee, S. G. Kim, H. J. Kim, and S. H. Ahn, “Measurement of anisotropic compressive strength of rapid prototyping parts,” *J. Mater. Process. Technol.*, vol. 187–188, pp. 627–630, 2007.

[12] W. C. Smith and R. W. Dean, “Structural characteristics of fused deposition modeling polycarbonate material,” *Polym. Test.*, vol. 32, no. 8, pp. 1306–1312, 2013.

[13] W. Zhong, F. Li, Z. Zhang, L. Song, and Z. Li, “Short fiber reinforced composites for fused deposition modeling,” *Mater. Sci. Eng. A301*, vol. 301, pp. 125–130, 2001.

[14] M. L. Shofner, F. J. Rodríguez-Macías, R. Vaidyanathan, and E. V. Barrera, “Single wall nanotube and vapor grown carbon fiber reinforced polymers processed by extrusion freeform fabrication,” *Compos. Part A Appl. Sci. Manuf.*, vol. 34, no. 12, pp. 1207–1217, 2003.

[15] M. Nikzad, S. H. Masood, and I. Sbarski, “Thermo-mechanical properties of a highly filled polymeric composites for Fused Deposition Modeling,” *Mater. Des.*, vol. 32, no. 6, pp. 3448–3456, 2011.

[16] H. L. Tekinalp, V. Kunc, G. M. Velez-Garcia, C. E. Duty, L. J. Love, A. K. Naskar, C. A. Blue, and S. Ozcan, “Highly oriented carbon fiber-polymer composites via additive manufacturing,” *Compos. Sci. Technol.*, vol. 105, pp. 144–150, 2014.

[17] F. Ning, W. Cong, J. Qiu, J. Wei, and S. Wang, “Additive manufacturing of carbon fiber reinforced thermoplastic composites using fused deposition modeling,” *Compos. Part B Eng.*, vol. 80, pp. 369–378, 2015.

[18] Z. Quan, Z. Larimore, A. Wu, J. Yu, X. Qin, M. Mirotznik, J. Suhr, J. H. Byun, Y. Oh, and T. W. Chou, “Microstructural design and additive manufacturing and characterization of 3D orthogonal short carbon fiber/acrylonitrile-butadiene-styrene preform and composite,” *Compos. Sci. Technol.*, vol. 126, pp. 139–148, 2016.

[19] O. S. Carneiro, A. F. Silva, and R. Gomes, “Fused deposition modeling with polypropylene,” *Mater. Des.*, vol. 83, pp. 768–776, 2015.

[20] R. T. L. Ferreira, I. C. Amatte, T. A. Dutra, and D. Bürger, "Experimental characterization and micrography of 3D printed PLA and PLA reinforced with short carbon fibers," *Compos. Part B Eng.*, vol. 124, no. September, pp. 88–100, 2017.

[21] J. Girdis, M. McCaffrey, and G. Proust, "Additive Manufacturing of Carbon Fiber Reinforced Thermoplastic Composites using Fused Deposition Modeling," *Solid Free. Fabr. 2016 Proc.*, no. 2010, pp. 864–870, 2016.

[22] P. Parandoush, L. Tucker, C. Zhou, and D. Lin, "Laser assisted additive manufacturing of continuous fiber reinforced thermoplastic composites," *Mater. Des.*, vol. 131, no. June, pp. 186–195, 2017.

[23] P. J. Hine, H. Rudolf Lusti, and A. A. Gusev, "Numerical simulation of the effects of volume fraction, aspect ratio and fibre length distribution on the elastic and thermoelastic properties of short fibre composites," *Compos. Sci. Technol.*, vol. 62, no. 10–11, pp. 1445–1453, 2002.

[24] X. Tian, T. Liu, C. Yang, Q. Wang, and D. Li, "Interface and performance of 3D printed continuous carbon fiber reinforced PLA composites," *Compos. Part A Appl. Sci. Manuf.*, vol. 88, pp. 198–205, Sep. 2016.

[25] R. Matsuzaki, M. Ueda, M. Namiki, T. K. Jeong, H. Asahara, K. Horiguchi, T. Nakamura, A. Todoroki, and Y. Hirano, "Three-dimensional printing of continuous-fiber composites by in-nozzle impregnation," *Sci. Rep.*, vol. 6, no. March, pp. 1–7, 2016.

[26] F. Van Der Klift, Y. Koga, A. Todoroki, M. Ueda, Y. Hirano, and R. Matsuzaki, "3D Printing of Continuous Carbon Fibre Reinforced Thermo-Plastic (CFRTP) Tensile Test Specimens," *Open J. Compos. Mater.*, vol. 06, no. 01, pp. 18–27, 2016.

[27] N. Li, Y. Li, and S. Liu, "Rapid prototyping of continuous carbon fiber reinforced polylactic acid composites by 3D printing," *J. Mater. Process. Technol.*, vol. 238, pp. 218–225, 2016.

[28] Y. Nakagawa, K. ichiro Mori, and T. Maeno, "3D printing of carbon fibre-reinforced plastic parts," *Int. J. Adv. Manuf. Technol.*, vol. 91, no. 5–8, pp. 2811–2817, 2017.

[29] P. Bettini, G. Alitta, G. Sala, and L. Di Landro, "Fused Deposition Technique for

Continuous Fiber Reinforced Thermoplastic," *J. Mater. Eng. Perform.*, vol. 26, no. 2, pp. 843–848, 2017.

[30] F. Zhang, P. Jiang, and Y. Tan, "Research on the Key Technology of Continuous Carbon Fiber Composite 3D Printinga," vol. 32, no. 4, pp. 619–625, 2017.

[31] T. H. J. Vaneker, "Material Extrusion of Continuous Fiber Reinforced Plastics Using Commingled Yarn," *Procedia CIRP*, vol. 66, pp. 317–322, 2017.

[32] M. Yamawaki and Y. Kouno, "Fabrication and mechanical characterization of continuous carbon fiber-reinforced thermoplastic using a preform by three-dimensional printing and via hot-press molding," *Adv. Compos. Mater.*, vol. 27, no. 2, pp. 209–219, 2018.

[33] A. N. Dickson, J. N. Barry, K. A. McDonnell, and D. P. Dowling, "Fabrication of continuous carbon, glass and Kevlar fibre reinforced polymer composites using additive manufacturing," *Addit. Manuf.*, vol. 16, pp. 146–152, 2017.

[34] Z. Hou, X. Tian, J. Zhang, and D. Li, "3D printed continuous fibre reinforced composite corrugated structure," *Compos. Struct.*, vol. 184, no. October, pp. 1005–1010, Jan. 2018.

[35] C. Yang, X. Tian, T. Liu, Y. Cao, and D. Li, "3D printing for continuous fiber reinforced thermoplastic composites: mechanism and performance," *Rapid Prototyp. J.*, vol. 23, no. 1, pp. 209–215, 2017.

[36] Y. Jin, Y. He, G. Fu, A. Zhang, and J. Du, "A non-retraction path planning approach for extrusion-based additive manufacturing," *Robot. Comput. Integr. Manuf.*, vol. 48, no. August 2016, pp. 132–144, Dec. 2017.

[37] B. K. Choi and R. B. Jerard, *Sculptured Machining*. .

[38] ASTM International, *F2792-12a - Standard Terminology for Additive Manufacturing Technologies*. 2013.

[39] E. Lee, "Contour offset approach to spiral toolpath generation with constant scallop height," *CAD Comput. Aided Des.*, vol. 35, no. 6, pp. 511–518, 2003.

[40] G. Elber, E. Cohen, and S. Drake, "C 1 continuous toolpath generation toward 5-axis high speed machining," *Comput. Aided. Des. Appl.*, vol. 3, no. 6, pp. 803–810, 2006.

[41] S. C. Park, Y. C. Chung, and B. K. Choi, “Contour-parallel offset machining without tool-retractions,” *CAD Comput. Aided Des.*, vol. 35, no. 9, pp. 841–849, 2003.

[42] M. Held, “A geometry-based investigation of the tool path generation for zigzag pocket machining,” *Vis. Comput.*, vol. 7, no. 5–6, pp. 296–308, 1991.

[43] M. Zhang, “Contour-parallel tool-path linking method without tool-retraction for complex-pocket,” *Comput. Integr. Manuf. Syst.*, vol. 16, pp. 1896–1901, 2010.

[44] K. Tang, S. Y. Chou, and L. L. Chen, “An algorithm for reducing tool retractions in zigzag pocket machining,” *CAD Comput. Aided Des.*, vol. 30, no. 2, pp. 123–129, 1998.

[45] W. S. W. Sheng, N. X. N. Xi, H. C. H. Chen, Y. C. Y. Chen, and M. S. M. Song, “Surface partitioning in automated CAD-guided tool planning for additive manufacturing,” *Proc. 2003 IEEE/RSJ Int. Conf. Intell. Robot. Syst. (IROS 2003) (Cat. No.03CH37453)*, vol. 2, no. October, pp. 2072–2077, 2003.

[46] R. Dwivedi and R. Kovacevic, “Automated torch path planning using polygon subdivision for solid freeform fabrication based on welding,” *J. Manuf. Syst.*, vol. 23, no. 4, pp. 278–291, 2004.

[47] M. Bertoldi, M. a Yardimci, C. M. Pistor, and S. I. Giiveri, “Domain Decomposition and Space Filling Curves in Toolpath Planning and Generation,” *Proceeeding 1998 Solid Fabr. Symp.*, pp. 267–276, 1998.

[48] D. Ding, Z. Pan, D. Cuiuri, and H. Li, “A tool-path generation strategy for wire and arc additive manufacturing,” *Int. J. Adv. Manuf. Technol.*, vol. 73, no. 1–4, pp. 173–183, 2014.

[49] H. Zhao, B. Chen, F. Gu, Q.-X. Huang, J. Garcia, Y. Chen, C. Tu, B. Benes, H. Zhang, and D. Cohen-Or, “Connected fermat spirals for layered fabrication,” *ACM Trans. Graph.*, vol. 35, no. 4, pp. 1–10, 2016.

[50] A. K. M. Khoda, I. T. Ozbolat, and B. Koc, “Designing heterogeneous porous tissue scaffolds for additive manufacturing processes,” *CAD Comput. Aided Des.*, vol. 45, no. 12, pp. 1507–1523, 2013.

[51] D. Joguet, Y. Danlos, R. Bolot, G. Montavon, and C. Coddet, “Modeling and Measurement of the Effective Young Modulus of Porous Biomedical Materials Manufactured via SLM,” vol. 606, pp. 125–128, 2014.